Paleoceanography and Paleoclimatology

RESEARCH ARTICLE
10.1029/2018PA003437

Key Points:
- Changes in western equatorial Atlantic thermocline depth were recorded on millennial and orbital time scales
- Shoaling of the thermocline during Heinrich stadials was associated with weak southeast trade winds
- Shoaling of the thermocline during periods of low-latitude boreal summer insolation maxima occurred due to decreased wind zonality

Supporting Information:
- Supporting Information S1
- Table S1
- Data Set S1

Correspondence to:
I. M. Venancio,
igor.venancio@inpe.br

Citation:
Venancio, I. M., Mulitza, S., Govin, A., Santos, T. P., Lessa, D. O., Albuquerque, A. L. S., et al. (2018). Millennial- to orbital-scale responses of western equatorial Atlantic thermocline depth to changes in the trade wind system since the Last Interglacial. *Paleoceanography and Paleoclimatology*, *33*. https://doi.org/10.1029/2018PA003437

Received 13 JUL 2018
Accepted 30 NOV 2018
Accepted article online 5 DEC 2018

Millennial- to Orbital-Scale Responses of Western Equatorial Atlantic Thermocline Depth to Changes in the Trade Wind System Since the Last Interglacial

I. M. Venancio[1,2], S. Mulitza[2], A. Govin[3], T. P. Santos[4], D. O. Lessa[2,4], A. L. S. Albuquerque[4], C. M. Chiessi[5], R. Tiedemann[6], M. Vahlenkamp[2], T. Bickert[2], and M. Schulz[2]

[1]Center for Weather Forecasting and Climate Studies (CPTEC), National Institute for Space Research (INPE), Cachoeira Paulista, Brazil, [2]MARUM—Center for Marine Environmental Sciences, University of Bremen, Bremen, Germany, [3]Laboratoire des Sciences du Climat et de l'Environnement/Institut Pierre Simon Laplace, CEA-CNRS-UVSQ, Université Paris-Saclay, Gif sur Yvette, France, [4]Programa de Pós-Graduação em Geoquímica Ambiental, Universidade Federal Fluminense, Niterói, Brazil, [5]School of Arts, Sciences and Humanities, University of São Paulo, São Paulo, Brazil, [6]Alfred Wegener Institute for Polar and Marine Research, Bremerhaven, Germany

Abstract Surface ocean circulation in the western equatorial Atlantic is mainly wind driven and plays a major role for the transport of warm waters to the North Atlantic. Past changes in the strength and direction of the trade winds are well documented, but the response of the western equatorial Atlantic circulation and water column structure to these changes is unclear. Here we used the difference between the stable isotopic oxygen composition of two species of planktonic foraminifera (*Globigerinoides ruber* white and *Neogloboquadrina dutertrei*) from two sediment cores collected off northeastern Brazil to investigate millennial- and orbital-scale changes in upper ocean stratification since the Last Interglacial. Our records indicate enhanced upper ocean stratification during several Heinrich stadials, partly due to a shoaling of the thermocline, which was linked to a decrease in the strength of southeast trades winds. In addition, we show that a decrease in wind zonality induced by increases in Northern Hemisphere low-latitude summer insolation causes a shoaling of the thermocline in the western equatorial Atlantic. These ocean-atmosphere changes contributed to a reduction in the cross-equatorial transport of warm waters, particularly during Heinrich stadials and Marine Isotope Stage 4.

1. Introduction

Trade winds form the lower limb of the Hadley circulation and are a dominant large-scale feature that influences continental climate and surface ocean circulation in the Atlantic (McGee et al., 2018). Blowing westward, these winds carry moisture to the Amazon basin and have a central role boosting the seasonal monsoon activity over South America (Marengo et al., 1993). Trade winds also have a major role on the transport and dispersal of African dust, which is considered to be a major aerosol source that influences the radiative balance over the Atlantic (Ridley et al., 2014). Over the ocean, trade winds push warm surface waters toward South America and pump cold and nutrient-rich deep waters to the surface on the vicinities of the African continent. This results in high-productivity areas offshore Namibia and Mauritania (Wefer & Fischer, 1993), while nutrient-depleted areas are commonly found in the western tropical Atlantic (Oudot et al., 1998).

In the equatorial Atlantic, relaxation or intensification of the trade winds influences the transport and pathway of the main ocean surface currents (Johns et al., 1998). For example, during boreal summer strengthened southeast (SE) trades cause an intensification of the South Equatorial Current (SEC) and consequently of the North Brazil Current (NBC), since the northern branch of the SEC feeds the NBC (Johns et al., 1998; Stramma et al., 1995). At the same time, increased westward wind stress produced by the strengthened SE trade winds piles up warm waters in the western and causes upwelling in the eastern equatorial Atlantic, producing an east-west asymmetry of the thermocline (Hastenrath & Merle, 1987). In addition, heat transported from the tropics and subtropics into the western equatorial Atlantic, which subsequently crosses the equator via the NBC, is increased during periods of strong SE trades (Johns et al., 1998; Kim et al., 2003). Part of this heat is deflected eastward by the NBC retroflection during boreal summer (Richardson & Reverdin, 1987). Thus, the trade winds not only create a thermocline asymmetry at the equator but also have an effect on cross-equatorial heat transport in the Atlantic.

Paleoclimate studies using multiple proxies (e.g., dust, sea surface temperature, and the relative abundance of planktonic foraminifera species) have shown that the trade wind system varied on millennial and glacial-interglacial timescales (Collins et al., 2013; Kim et al., 2003; Little et al., 1997; Stuut et al., 2002), which probably affected the upper ocean circulation and stratification in the equatorial Atlantic. In the western tropical Atlantic, planktonic foraminifera assemblages from gravity cores led Wolff et al. (1999) to suggest that glacial-interglacial changes of the thermocline depth were primarily driven by the strength of the SE trade winds. Other studies, using coccolithophores (Kinkel et al., 2000) and the oxygen-isotopic difference of planktonic foraminifera species (Rühlemann et al., 2001), reconstructed the thermocline depth in the western equatorial Atlantic and supported the mechanism described by Wolff et al. (1999). However, these previous works in the western equatorial Atlantic could not explore millennial-scale changes of the thermocline depth due to the low resolution of their records. Recently, a high-resolution record of planktonic foraminifera assemblages covering the last 30 ka, indicated that a shallow mixed layer depth occurred in the western equatorial Atlantic during Heinrich stadials (HS) 2 and 1, as well as the Younger Dryas (YD; Portilho-Ramos et al., 2017). The authors proposed that the increased stratification was linked to the excess of freshwater flux below the Intertropical Convergence Zone (ITCZ) that hinders wind-driven vertical mixing. In the eastern equatorial Atlantic, the direction (zonal vs. meridional) of the trade winds is considered as a main driver of past precession-related upper ocean changes in the eastern tropical Atlantic (McIntyre et al., 1989; Molfino & McIntyre, 1990), which probably influenced the westward transport of waters and consequently the upper ocean stratification in the western margin. However, Wolff et al. (1999) suggested that thermoclines in the eastern and western tropical Atlantic are dominated by different periodicities and ocean-atmosphere interactions. Therefore, a paleoceanographic investigation that addresses the changes in ocean stratification in the equatorial Atlantic on millennial and orbital timescales, considering all the plausible mechanisms, is still needed.

We present high-resolution reconstructions of the thermocline depth using two sediment cores (GL-1248 and GeoB16202-2) from the continental slope off northeastern Brazil, extending back to the Last Interglacial (LIG). We use the difference between the stable oxygen isotopic composition ($\delta^{18}O$) of two planktonic foraminifera species (*Globigerinoides ruber* white and *Neogloboquadrina dutertrei*; $\Delta\delta^{18}O_{dut\text{-}rub}$) as a proxy for past upper water column stratification or thermocline depth. We compare our results with other records from the eastern and western Atlantic to address the large-scale responses of upper ocean stratification on millennial and orbital timescales. Our results indicate a shoaling of the thermocline depth in the western equatorial Atlantic during Heinrich stadials, as a consequence of reduced westward transport of warm waters due to a weakening of the SE trade winds. Furthermore, spectral analysis performed on our $\Delta\delta^{18}O_{dut\text{-}rub}$ records shows significant periodicities in the 19- to 23-kyr frequency band, which supports a response of upper ocean stratification to precessional forcing.

2. Background

2.1. Regional Setting

Modern surface ocean circulation in the western equatorial Atlantic is dominated by the northwestward-flowing NBC, which transports warm and salty waters to the North Atlantic (Figure 1). The NBC originates from the northern branch of the SEC bifurcation around 10°S (Stramma et al., 1995) and has an annual mean transport of approximately 26 Sv (Johns et al., 1998). Seasonal variability of the NBC transport is linked to changes in the trade wind system and ITCZ position. During boreal summer and fall, when SE trade winds are strong (Figure 2a), a maximum transport of 36 Sv of the NBC is observed (Johns et al., 1998). Such intensification of the NBC is partially due to the southernmost position of the SEC bifurcation, which is in turn associated with the northward displacement of the ITCZ (Rodrigues et al., 2007). At the same time, the NBC keeps its main route, flowing northwestward, until it reaches 6–7°N where it retroflects (Johns et al., 1998) and feeds the North Equatorial Counter Current (NECC). The NECC transports surface waters eastward (Richardson & Reverdin, 1987), causing a deepening of the thermocline along its pathway (Figure 2e). At the NBC retroflection, large anticyclonic eddies known as NBC rings are detached and are responsible for the northward transport of heat and mass (Goni & Johns, 2001). Also, during this period, the SEC transport increases, piling up warm waters and consequently deepening the thermocline in the western equatorial Atlantic (Hastenrath & Merle, 1987; Figures 2c and S1 in the supporting information). During boreal winter and spring, the northeast (NE) trade winds are strong, and the NBC transport decreases to 13 Sv (Johns et al., 1998). The

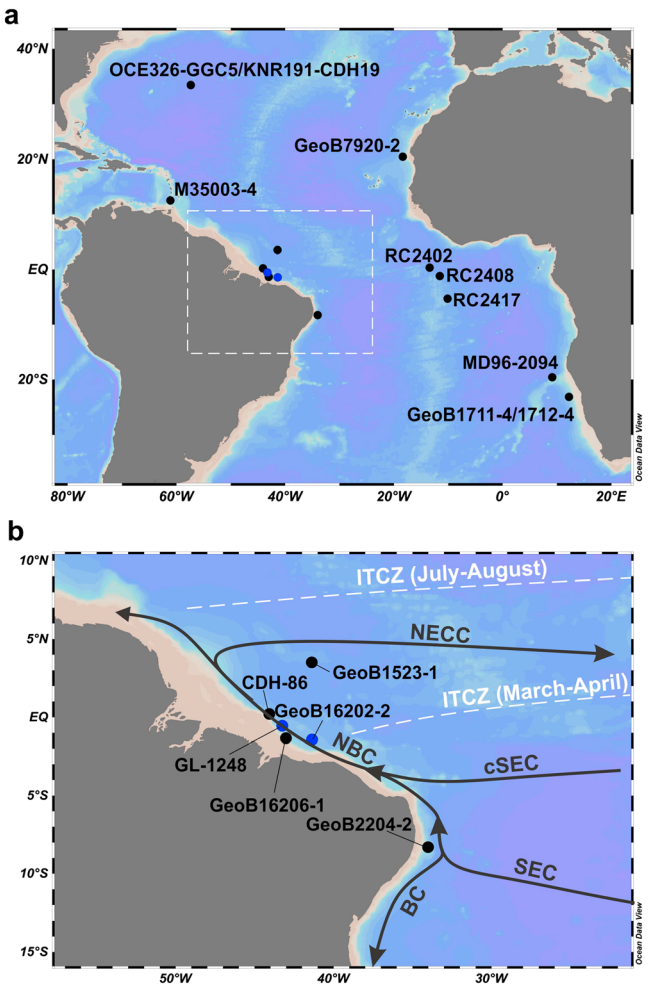

Figure 1. Location of the studied cores and other records discussed in the text. (a) Cores GL-1248 and GeoB16202-2 (blue dots) analyzed in this study together with the following cores discussed in the text (black dots): OCE326-GGC5 (McManus et al., 2004), KNR191-CDH19 (Henry et al., 2016), MD96-2094 (Stuut et al., 2002), GeoB1711-4 (Kirst et al., 1999; Little et al., 1997), GeoB7920-2 (Collins et al., 2013), M35003-4 (Hüls & Zahn, 2000), RC2402/RC2408/RC2417 (McIntyre & Molfino, 1996). The dashed white rectangle marks the area enlarged in panel b. (b) Besides cores GL-1248 and GeoB16202-2, the other cores in the western equatorial Atlantic are GeoB2204-2 (Wolff et al., 1999), GeoB1523-1 (Kinkel et al., 2000), CDH-86 (Nace et al., 2014), and GeoB16206-1 (Portilho-Ramos et al., 2017). Black solid lines with arrows indicate surface currents and white dotted lines the seasonal range of the Intertropical Convergence Zone (ITCZ). The surface currents shown are the Brazil Current (BC), North Brazil Current (NBC), North Equatorial Countercurrent (NECC), and the southern and central branches of the South Equatorial Current (SEC and cSEC, respectively). The figure was generated using the software Ocean Data View (Schlitzer, 2017).

SEC bifurcation moves north, when the ITCZ is at its southernmost position, contributing to a reduction in the NBC transport (Rodrigues et al., 2007). During this time, the NBC retroflection and the NECC are weak (or not present), which favors the NBC northwestward flow along the continental margin of South America (Hastenrath & Merle, 1987; Stramma et al., 1995; Figure 2b). In addition, the east-west pressure gradient and thermocline tilt weaken (Figure 2d), smoothing out the latitudinal variations in thermocline depth across the equator (Figure 2f). The southward migration of the ITCZ during this period, especially between March and April, characterizes the rainy season over northeastern Brazil (Hastenrath, 2012).

Seasonal changes in upper water column stratification and thermocline depth in the western equatorial Atlantic are connected to variations in surface ocean circulation, which are in turn influenced by the strength and direction (zonal vs. meridional) of the trade winds (Hastenrath & Merle, 1987). The strength of the trade winds depends on the atmospheric pressure gradients, which are modulated by meridional SST gradients in the ocean (Rind, 1998). Thus, during boreal winter (summer), the SE trade winds are weak (strong), and the SEC transport of warm waters to the western equatorial Atlantic decreases (increases), which causes a relaxation (accentuation) of the east-west thermocline tilt and consequently a shoaling (deepening) of the thermocline in the west (Figures 2a–2d).

2.2. Upper Ocean Stratification Recorded by Interspecific Planktonic Foraminiferal Oxygen Isotopic Composition

One of the most widely used planktonic foraminiferal proxies to reconstruct the upper ocean stratification (or thermocline depth) is the difference in oxygen isotopic composition between surface and thermocline species. This proxy can be applied using shallow and deep-dwelling planktonic foraminiferal species (Mulitza et al., 1997; Williams & Healy-Williams, 1980) and requires knowledge of the calcification depths of the chosen species. Studies using core top $\delta^{18}O$ values of *G. ruber* (white) and *N. dutertrei* in the western tropical Atlantic have estimated the apparent calcification depths of both species (Cléroux et al., 2013; Farmer et al., 2007; Steph et al., 2009). These studies show that *G. ruber* (white) $\delta^{18}O$ records the conditions within the mixed layer, calcifying around 16 m as estimated by Farmer et al. (2007), or around 89 m as suggested by Steph et al. (2009), where the difference between these estimations can be attributed to distinct methodologies used by these studies. On the other hand, *N. dutertrei* $\delta^{18}O$ records the upper thermocline with apparent average calcification depths varying between 104 and 118 m (Cléroux et al., 2013; Farmer et al., 2007; Steph et al., 2009).

Here we first verify the apparent calcification depth of both planktonic foraminifera species at our core sites. We compare the core top calcite $\delta^{18}O$ values ($\delta^{18}O_c$) measured for both species in cores GL-1248 and GeoB16202-2 to the predicted $\delta^{18}O_c$ profile at our core sites. We use the nearest temperature and salinity profiles (0.5°S, 43.5°W) from the World Ocean Atlas (2013; Locarnini et al., 2013) to derive the vertical profile of predicted $\delta^{18}O_c$. First, the $\delta^{18}O$ of seawater ($\delta^{18}O_{sw}$) was calculated from the salinity profile using the salinity-$\delta^{18}O_{sw}$ relationship suggested by Regenberg et al. (2009) for the tropical Atlantic. The $\delta^{18}O_{sw}$ values were converted from Vienna Standard Mean Ocean Water to Vienna Pee Dee Belemnite by subtracting 0.27‰ (Hut, 1987). Then, a profile of the predicted $\delta^{18}O$ of the calcite was generated for each species at the core sites by applying paleo-temperature equations to the water column temperature and the estimated $\delta^{18}O_{sw}$ profiles. For *G. ruber* (white) we applied the equation of Mulitza

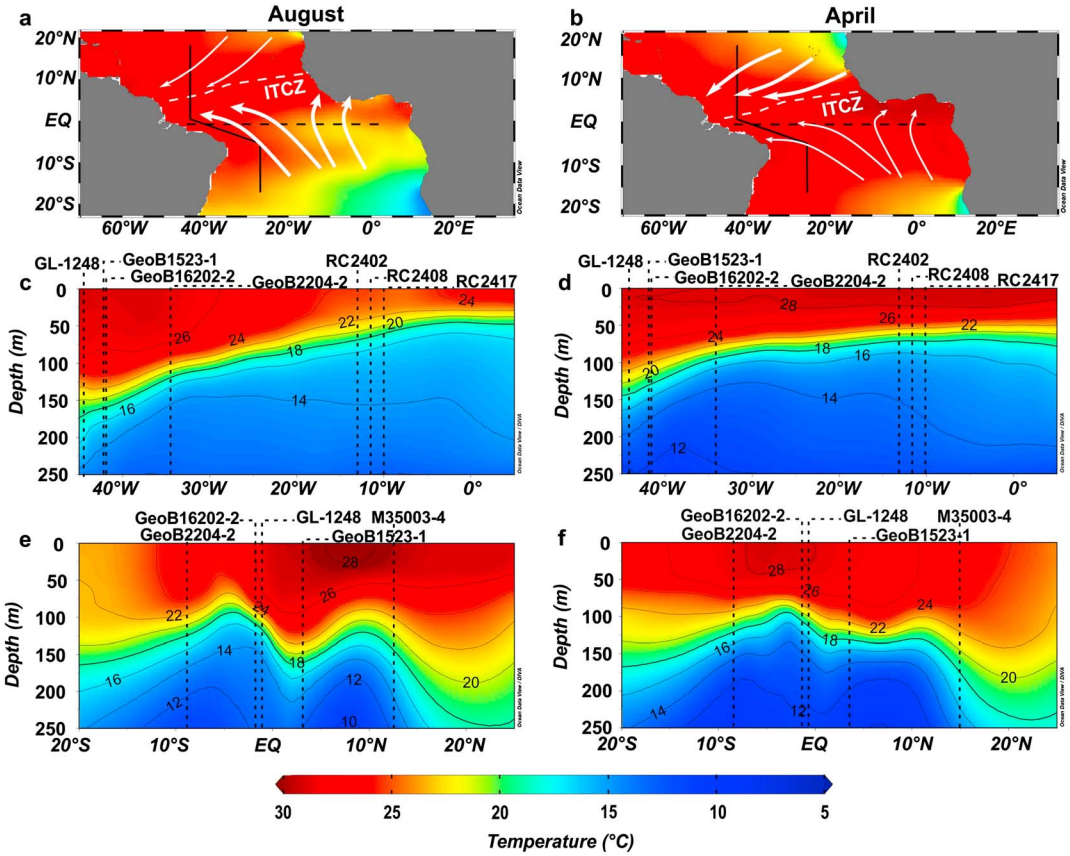

Figure 2. August and April mean states of the tropical wind system and thermal stratification. (a and b) Seasonal variation of the Intertropical Convergence Zone (ITCZ) position (white dotted line), as well as of the northeast and southeast trade winds (white arrows), where the relative strength of the winds is represented by the thickness of the lines. (c and d) Upper Atlantic temperature distribution during August (c) and April (d) on a longitudinal transect along the equator (black dashed line in panels a and b). (e and f) Upper Atlantic temperature distribution during August (e) and April (f) on a latitudinal transect (black solid line panels a and b). The position of the cores considered in this study relative to the temperature distribution depicted in the transects is shown with vertical dotted lines in panels c to f. Data are from the World Ocean Atlas (2013; Locarnini et al., 2013). The figure was generated using the software Ocean Data View (Schlitzer, 2017).

et al. (2003) for this species, and for *N. dutertrei* we applied the equation from Bemis et al. (1998) for *O. universa* (culture-low light). We chose not to apply the species-specific equation for *N. dutertrei* from Bouvier-Soumagnac and Duplessy (1985), because the coefficients of this equation show large errors and the equation was built in a narrow temperature range (24–30 °C; Wejnert et al., 2013), which does not represent the vertical temperature range at our sites. The projection of the measured core top $\delta^{18}O_c$ values onto the predicted $\delta^{18}O_c$ profile shows that, indeed, *G. ruber* (white) has an apparent calcification depth within the mixed layer, while *N. dutertrei* has an apparent calcification depth between 100 and 150 m at both sites (Figure 3). This result is in agreement with previous studies (Cléroux et al., 2013; Farmer et al., 2007; Steph et al., 2009).

The $\delta^{18}O$ difference between *G. ruber* (white) and *N. dutertrei* ($\Delta\delta^{18}O_{dut\text{-}rub}$) should track the latitudinal and longitudinal changes in thermocline depth in the tropical Atlantic (Figures 2c–2f). Therefore, we used published core top $\delta^{18}O$ values (Arbuszewski et al., 2010; Cléroux et al., 2013; Steph et al., 2009) to calculate values for $\Delta\delta^{18}O_{dut\text{-}rub}$ along one latitudinal and one longitudinal transect (Figure S2). The results show that $\Delta\delta^{18}O_{dut\text{-}rub}$ reproduces relatively well the modern upper ocean stratification in the tropical Atlantic. In the latitudinal transect, the $\Delta\delta^{18}O_{dut\text{-}rub}$ values indicate a deep thermocline close to the subtropical gyres on both hemispheres and a shallow thermocline around the equator (Figure S2a). This proxy is even sensitive to slight deepening of the thermocline observed around 0–5°N (Figure S2a), which is probably due to the influence of the NECC, or of the NBC retroflection. Furthermore, despite the scatter of data points, the $\Delta\delta^{18}O_{dut\text{-}rub}$ seems to capture the thermocline tilt between the eastern and western tropical Atlantic (Figure S2b).

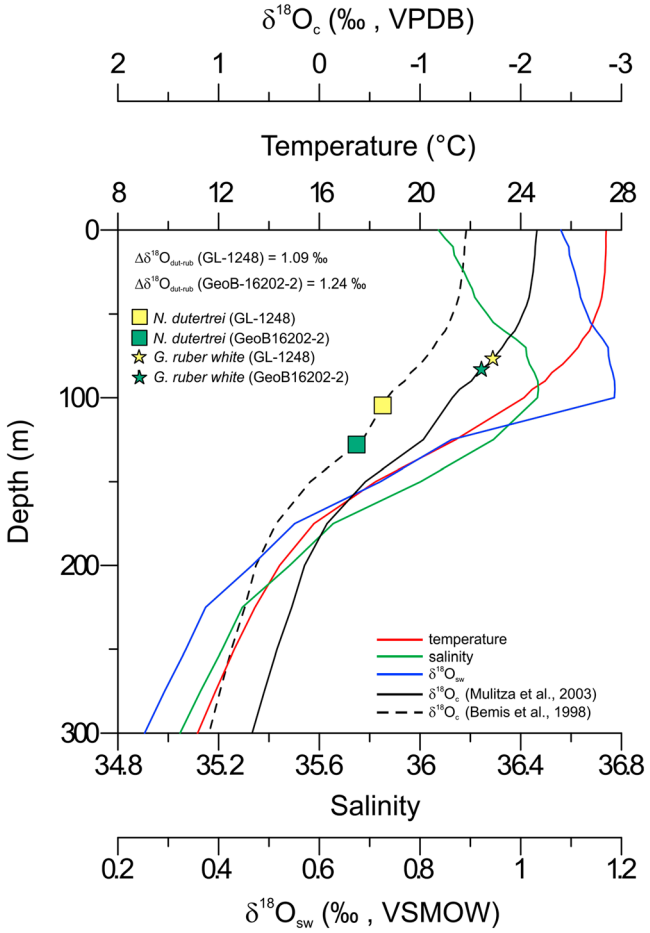

Figure 3. Oceanographic profile from the World Ocean atlas (2013) (Locarnini et al., 2013) at 0.5°S, 43.5°W, near to the position of cores GL-1248 and GeoB16202–2, with temperature (red line), salinity (green line) and the estimated $\delta^{18}O$ values of seawater ($\delta^{18}O_{sw}$,blue line). The predicted $\delta^{18}O$ of the calcite ($\delta^{18}O_c$, black line) was estimated using the paleotemperature equations from Mulitza et al. (2003) (solid line) for *G. ruber* (white) and the equation from Bemis et al. (1998) (dotted line) for *O. universa* (culture-low light). The measured $\delta^{18}O$ core top values of *G. ruber* white (star symbols) and *N. dutertrei* (square symbols) for GL-1248 (yellow symbols) and GeoB16202–2 (green symbols) were plotted on the $\delta^{18}O_c$ vertical profiles in order to estimate the apparent calcification depths of the two species at the core sites.

Finally, core top (0–2 cm) $\Delta\delta^{18}O_{dut\text{-}rub}$ values of 1.09‰ and 1.24‰ were calculated for cores GL-1248 and GeoB16202-2, respectively. These values are close to the range of regional $\Delta\delta^{18}O_{dut\text{-}rub}$ values from other core tops (Figure S2). Thus, assuming that the calcification depths of *G. ruber* (white) and *N. dutertrei* are constant through time, high $\Delta\delta^{18}O_{dut\text{-}rub}$ values mean a shallow thermocline and a strong upper ocean stratification between the surface and the thermocline, while low $\Delta\delta^{18}O_{dut\text{-}rub}$ values imply the opposite oceanographic conditions.

3. Material and Methods

3.1. Location and Lithology of Sediment Cores

Sediment core GL-1248 (0°55.2′S, 43°24.1 ′W, 2,264-m water depth, 19.29 m long) was retrieved by Petrobras on the continental slope off northeastern Brazil, 170 km from the coastline and 280 km to the north of the mouth of the Parnaíba River (Figure 1). Between 1.00–12.99 m and 16.60–19.29 m, core GL-1248 consists mainly of greenish to olive sediments, which are rich in silty clay. GL-1248 contains carbonate-rich sediments between 0–1.00 m and 12.99 to 16–60 m, which are represented by more reddish-brown and whitish clays. Sediment core GeoB16202–2 (1°54.50′S, 41°35.50′W, 2,248-m water depth, 7.73 m long) was taken during the cruise MSM20/3 (Mulitza et al., 2013) also from the continental slope off northeastern Brazil, 92 km from the coastline and 101 km to the north of the Parnaíba River mouth (Figure 1). The entire lithology of GeoB16202-2 consists of clay-rich sediments with colors varying between greenish gray and dark olive.

3.2. Stable Oxygen Isotopes

Ten tests of *G. ruber* (white; 250–355 μm) and eight tests of *N. dutertrei* (350–415 μm) were analyzed for $\delta^{18}O$ every ~4 cm of core GL-1248 from the top of the core until 16.60 m. For core GeoB16202-2, five to 10 tests of *G. ruber* (white; 350–500 μm) and a sufficient number of tests of of *N. dutertrei* (350–450 μm) were selected every ~10 cm and analyzed for $\delta^{18}O$ (Huppertz, 2014). All tests were handpicked under a binocular microscope. Stable oxygen isotope analyses were performed with a Finnigan MAT 252 mass spectrometer equipped with an automatic carbonate preparation device at MARUM, University of Bremen (Germany). Isotopic results were calibrated relative to the Vienna Pee Dee Belemnite using the standards NBS18, 19 and 20. The standard deviation of the laboratory standard was lower than 0.07‰ for the measuring period.

3.3. Major Element Composition

The Ti and Ca intensities of core GL-1248 were obtained by scanning the core surface of the archive half with X-ray fluorescence Core Scanner II (AVAATECH Serial No. 2) at the MARUM, University of Bremen (Germany). The X-ray fluorescence data were measured downcore every 0.5 cm for GL-1248 by irradiating a surface of about 10 mm × 12 mm for 20 s at 10 kV. This analysis allows the determination of Ti/Ca ratios for core GL-1248, which similarly to Fe/Ca ratios is a well establish proxy for terrigenous input of fluvial origin offshore northeastern Brazil (Arz et al., 1998; Govin et al., 2012; Jaeschke et al., 2007; Mulitza et al., 2017; Zhang et al., 2015). Millennial-scale maxima in Ti/Ca ratios reflects enhanced erosion and fluvial transport of terrigenous material to the ocean, occurring during periods characterized by abrupt increases in precipitation on the adjacent continent (Arz et al., 1998; Jaeschke et al., 2007).

3.4. Age Model

The age model for core GeoB16202-2 is based on 13 AMS radiocarbon ages performed on two shallow-dwelling planktonic foraminifera species (*G. ruber* and *Trilobatus sacculifer)* measured at the Poznań

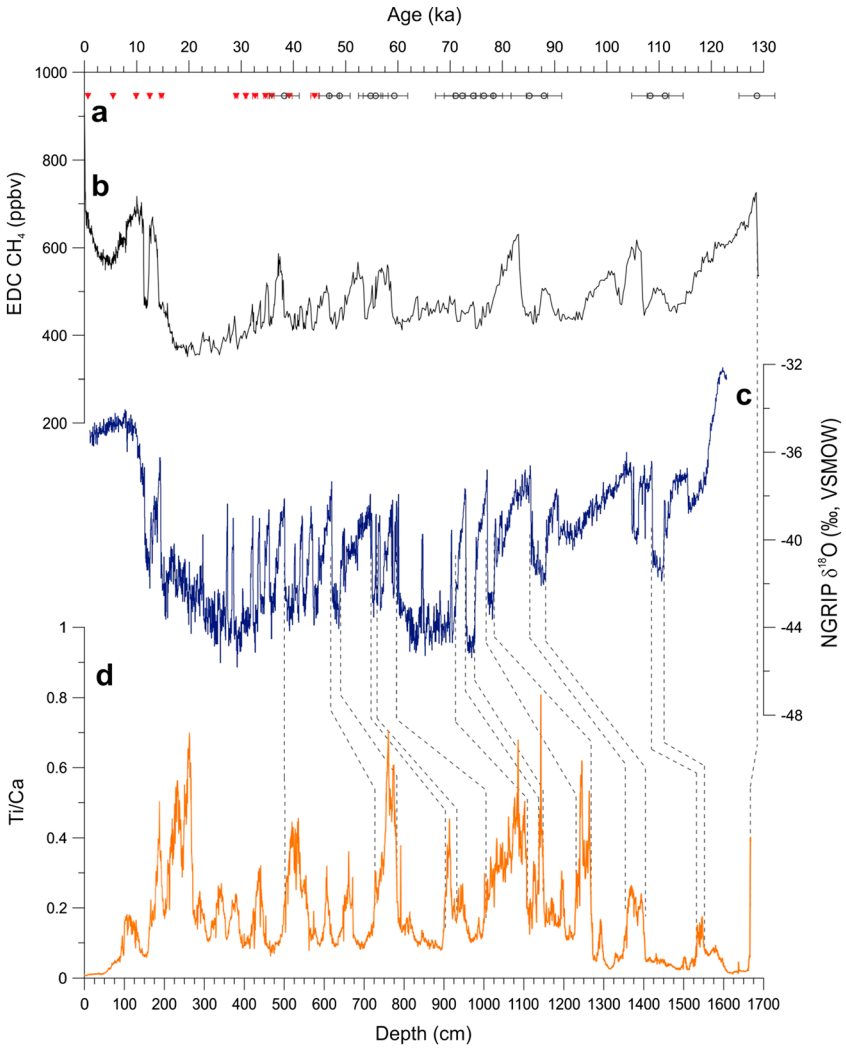

Figure 4. Reference curves and age–depth model of core GL-1248. (a) Calibrated radiocarbon dates (red symbols) and tie-points (open circles) with their respective 2σ errors. (b) EPICA dome C (EDC) methane record (Loulergue et al., 2008) on the AICC2012 timescale (Veres et al., 2013) (black line). (c) $\delta^{18}O_{ice}$ from NGRIP on the GICC05modelext time scale (NGRIP members, 2004; Wolff et al., 2010; blue line). (d) Ti/ca record from GL-1248 versus core depth (orange line). The black dotted lines represent the tie-point alignment.

Radiocarbon Laboratory (Mulitza et al., 2017). Downcore ages were modeled using BACON software version 2.2 (Blaauw & Christen, 2011) and the radiocarbon ages were calibrated with the IntCal13 calibration curve (Reimer et al., 2013) with a reservoir age of 400 ± 200 years (2σ) and no additional local reservoir effect (ΔR = 0; Mulitza et al., 2017). The age model for core GL-1248 is based on 12 AMS radiocarbon ages for the upper 6.30-m core depth. Two age reversals at 278 and 322 cm were not included and may be due to the presence of dark material inside some planktonic foraminifera shells, which probably contained older carbonate fragments derived from reworked material. Each radiocarbon sample contained about 400–500 tests of *G. ruber* and *T. sacculifer* handpicked from the fraction larger than 150 μm. Samples were analyzed at the Beta Analytic Radiocarbon Dating Laboratory, USA. For the sake of consistency and comparison between data from core GeoB16202-2 and GL-1248, we used the same calibration curve, reservoir age, and local reservoir effect used for GeoB16202-2 for the age model of core GL-1248, but downcore ages were modeled using the software clam 2.2 (Blaauw, 2010).

For the lower part of core GL-1248 (6.30- to 16.66-m core depth; ≈44–129 ka), the chronology was derived from the alignment of the Ti/Ca record of core GL-1248 to the ice $\delta^{18}O$ (Figure 4) record of the North Greenland Ice Core Project (NGRIP) using the extended Greenland Ice Core Chronology (GICC05modelext)

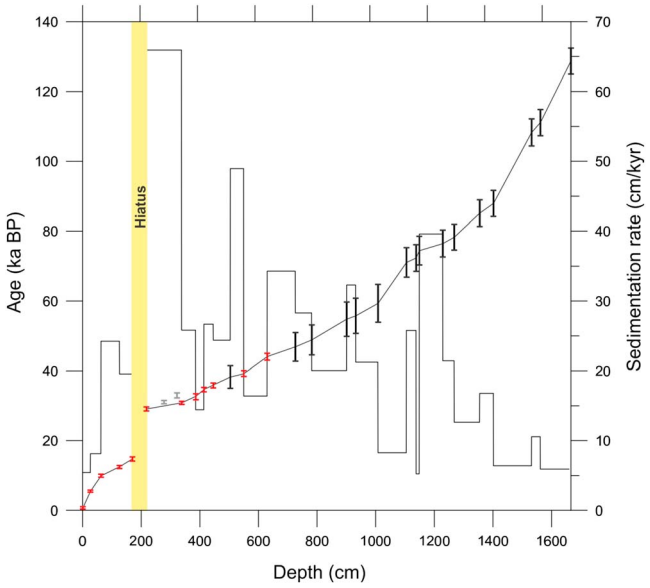

Figure 5. Age-depth model and sedimentation rates for core GL-1248. Vertical error bars denote 2σ confidence interval of the calibrated ages (red), tie points (black), and age reversals (gray). The gray line represents the age-depth model constructed based on the linear interpolation between adjacent calibrated radiocarbon ages and tie points. The step plot shows the changes in sedimentation rate based on the median values of the calibrated ages. The yellow bar shows the position of a hiatus.

(NGIRP members, 2004; Wolff et al., 2010). The underlying assumption to this alignment is that Greenland stadials are associated with increased precipitation over northeastern Brazil and increased delivery of terrigenous material to the western equatorial Atlantic, as supported by speleothem and marine records of the last glacial period (e.g., Jaeschke et al., 2007; Wang et al., 2004; Zhang et al., 2017). Thus, the major Ti/Ca fluctuations of core GL-1248 were matched with the major changes in $\delta^{18}O$ from the NGRIP record, with tie points being mostly located at the midpoint of abrupt excursions on both records. In addition, the onset of the LIG was defined by aligning the Ti/Ca record of core GL-1248 with the Antarctic methane record from EPICA Dome C (Loulergue et al., 2008) at approximately 129 ka on the AICC2012 timescale (Veres et al., 2013), similarly to previous studies (e.g., Govin et al., 2015). The rationale behind this alignment is that abrupt Greenland warming events occurred simultaneously with methane increases during millennial-scale events of the last glacial period and the last deglaciation (Baumgartner et al., 2014; Chappellaz et al., 1993; Huber et al., 2006). We estimated the error for the defined tie points by taking into account (1) the mean resolution of the Ti/Ca record from GL-1248, (2) the mean resolution and dating uncertainty of the reference curves, and (3) an estimated matching error when defining a tie point. Since the GICC05modelext chronology does not have an intrinsic age error estimate between 60 and 123 ka, we assumed that the errors from GICC05modelext are similar to AICC2012 (Veres et al., 2013). The complete age model was constructed using linear interpolation with the software clam 2.2 (Blaauw, 2010), where we used the median values of the calibrated age distributions. Then, using the same approach as Jaeschke et al. (2007), we used U/Th-dated growth intervals of Brazilian speleothems during stadials (Wang et al., 2004) to verify our age model (Figure S4). Since these growth intervals correspond to wet periods in northeastern Brazil, synchronous with cold events (stadials) in the North Atlantic, they should be coeval to the Ti/Ca peaks in our record. Radiocarbon ages and tie points defined for GL-1248 with their respective 2σ errors are summarized in Table S1.

To assess the uncertainty in the $\delta^{18}O$ difference between *G. ruber* and *N. dutertrei*, we drew 10,000 ages from probability density functions of each of the age-control point and combined the resulting age model ensemble with an ensemble of 10,000 noisy downcore proxy series representing the analytical uncertainty of 0.07‰ (1 SD). The resulting 10,000 time series were interpolated to the mean of all ages at each depth where stable isotopes have been measured to estimate the 95% confidence margin (i.e., Breitenbach et al., 2012).

Core GeoB16202-2 reaches 23.9 ka (± 0.6) close to its base at 7.63-m core depth (Mulitza et al., 2017). For core GL-1248, radiocarbon dating suggest an age of about 44.0 ± 0.7 ka at 6.30-m core depth, and the bottom age is 128.7 ka at 16.66-m core depth (Figure 5). The very low sedimentation rate (≈3 cm/kyr) between 2.18- and 1.70-m core depth (29.1 and 14.8 ka, respectively) is unusual for this region and period (see Zhang et al., 2015), suggesting the presence of a hiatus, even though no significant change in lithology is observed; thus, the data of GL-1248 within this interval was not interpreted. A potential driver of this hiatus could be local changes in depocenters due to variations in sea level and ocean currents strength during the Last Glacial Maximum (LGM) and Termination I. Outside the hiatus interval, the mean sedimentation rate for GL-1248 is 21 cm/kyr, with higher values reaching 67 cm/kyr during Marine Isotope Stage 3 (MIS3) and lower values under 10 cm/kyr during MIS1 and MIS5. Finally, the peaks in Ti/Ca from core GL-1248 coincide with the U/Th-dated growth intervals of Brazilian speleothems during stadials (Wang et al., 2004), which supports our age model for core GL-1248 (Figure S3).

3.5. Time Series Analysis

In order to test for the presence of periodicities in our data set, spectral analysis was performed. The $\Delta\delta^{18}O_{dut\text{-}rub}$ composite (GeoB16202-2/GL-1248) was analyzed using the REDFIT algorithm (Schulz & Mudelsee, 2002) as implemented in the software PAST (Hammer et al., 2001). This algorithm allows us to

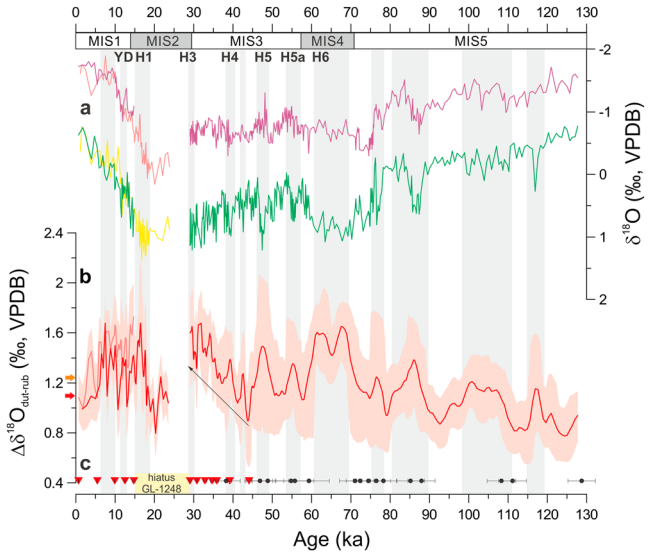

Figure 6. Stable oxygen isotopic results from cores GL-1248 and GeoB16202-2. (a) $\delta^{18}O$ of *Globigerinoides ruber* (white) and *Neogloboquadrina dutertrei* from GeoB16202-2 (pink and yellow lines, respectively) and from GL-1248 (purple and green lines, respectively). (b) Monte Carlo ensemble mean $\Delta\delta^{18}O_{dut\text{-}rub}$ values from both cores, GeoB16202-2 (red line) and GL-1248 (red line for the lower part and light red line for the upper part of the record). Shadings with the same color code indicate the 95% confidence envelope including age and analytical uncertainties. The arrows represent the $\Delta\delta^{18}O_{dut\text{-}rub}$ core top values for core GeoB16202-2 (orange) and GL-1248 (red). (c) Calibrated radiocarbon ages (red inverted triangles) and tie points (black circles) with their respective 2σ errors are displayed above the lower *x*-axis. Gray bars highlight the peaks in $\Delta\delta^{18}O_{dut\text{-}rub}$. The Younger Dryas (YD) and Heinrich Stadials (HS) are marked close to the upper *x*-axis. Black arrow highlights a trend during late MIS 3 in the $\Delta\delta^{18}O_{dut\text{-}rub}$. The hiatus in core GL-1248 is marked with a yellow rectangle close the lower *x*-axis. Marine isotope stages (MIS) are highlighted below the upper *x*-axis.

work directly with unevenly spaced data, avoiding the introduction of bias during interpolation (Schulz & Mudelsee, 2002). For this analysis, a setting of three segments tapered with a Welch spectral window was selected, the oversampling factor was set to 4, and the data were linearly detrended with the software PAST. Spectral peaks exceeding the false-alarm level of Thomson (1990) as well as 95% and 99% were considered during the interpretation of the results.

4. Results

4.1. Stable Oxygen Isotopes

The *G. ruber* (white) $\delta^{18}O$ values vary between −1.74‰ and 0.00‰ in core GeoB16202-2 and between −1.80‰ and −0.29‰ in core GL-1248 (Figure 6a). *N. dutertrei* $\delta^{18}O$ values range from −0.76‰ to 1.37‰ in core GeoB16202-2 and from −0.77‰ to 1.22‰ in core GL-1248. Oxygen isotopic values for both cores overlap over the last 14.5 ka with good agreement (Figure 6a).

High $\Delta\delta^{18}O_{dut\text{-}rub}$ values, which indicate increased upper ocean stratification, were observed during several time intervals (Figure 6b). During MIS5, wide peaks between 110–100 ka and 90–80 ka, as well as short peaks (centered near 117 and 77 ka) in $\Delta\delta^{18}O_{dut\text{-}rub}$ values of core GL-1248, are present with values higher than 1.0‰. From MIS5 to MIS4, a long-term increase in the $\Delta\delta^{18}O_{dut\text{-}rub}$ values of core GL-1248 can be observed. During MIS4, the $\Delta\delta^{18}O_{dut\text{-}rub}$ values of core GL-1248 are generally higher than 1.2‰. The two distinguishable peaks in $\Delta\delta^{18}O_{dut\text{-}rub}$ during MIS4 (centered near 68 and 62 ka) are divided by a short-time decrease in $\Delta\delta^{18}O_{dut\text{-}rub}$ at 65 ka. For MIS3, abrupt increases can be observed in the $\Delta\delta^{18}O_{dut\text{-}rub}$ of core GL-1248, where the most pronounced increases occurred around 55, 48, 42, and 39 ka. The peaks centered near 42 and 39 ka appear to be part of a long-term trend (Figure 6b) during the late MIS3 (47–30 ka). In core GeoB16202–2, low $\Delta\delta^{18}O_{dut\text{-}rub}$ values (< 1.1 ‰) are present during the LGM. During the deglacial, the highest $\Delta\delta^{18}O_{dut\text{-}rub}$ value (2.12 ‰) in core GeoB16202-2 is observed near 17 ka and a minor peak in $\Delta\delta^{18}O_{dut\text{-}rub}$ is present in both cores around 12.6 ka. In the Holocene, high $\Delta\delta^{18}O_{dut\text{-}rub}$ values were observed for the Early Holocene (EH; 10–8 ka) on both cores, subsequently decreasing toward the present.

During several of the mentioned periods of increased stratification, the values of $\delta^{18}O$ of *G. ruber* (white) decreased, and the values of *N. dutertrei* increased (Figures 6a and S4). However, exceptions to this pattern are observed: (1) during the EH, with no clear increase in $\delta^{18}O$ values of *N. dutertrei* in both cores; (2) during the late MIS3 (47–30 ka), where a trend toward high values of $\delta^{18}O$ is observed for *N. dutertrei* and no trend is present in $\delta^{18}O$ values of *G. ruber* (white) from core GL-1248; and (3) for the cold substages of MIS5 (110–95 and 90–80 ka), where the $\delta^{18}O$ values of both species coeval in core GL-1248 but a larger increase in $\delta^{18}O$ values of *N. dutertrei* is observed (Figure 6b). Data from cores GL-1248 and GeoB16202-2 is available in Data Set S1. Finally, the combined use of data from both cores for the next sections is supported by the fact that isotopic data from these cores show good agreement over the last 14.5 ka, the two cores are under the influence of the NBC, and they receive terrigenous material from the Parnaíba River, as evidenced by cores nearby (Nace et al., 2014; Zhang et al., 2015).

4.2. Time Series Analysis

The $\Delta\delta^{18}O_{dut\text{-}rub}$ composite record (GeoB16202-2/GL-1248) revealed the presence of short- and long-term periodicities (Figure 7). The results show the presence of a periodicity centered at 19.5 ka (21.1–16.9 ka) with a high spectral power and above the 99.5% false-alarm level (after Thomson, 1990). Other periodicities centered near 7.4, 4.4, 2.6, and 0.8 ka can also be observed above the 95% level.

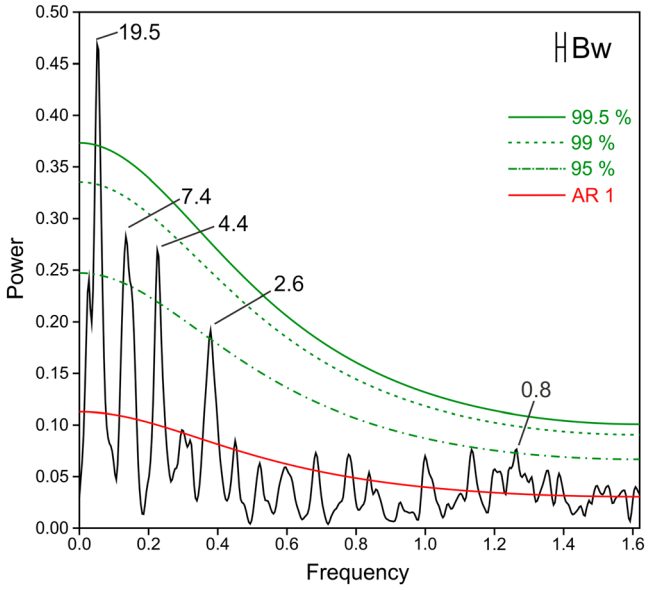

Figure 7. Spectral analysis performed on the $\Delta\delta^{18}O_{dut\text{-}rub}$ composite (GeoB16202-2/GL-1248) with the REDFIT algorithm (Schulz & Mudelsee, 2002). The red line represents the red-noise spectrum, and the green lines show the false-alarm levels at 95% (dot-dashed line), 99% (dashed line), and 99.5% (after Thomson, 1990; solid line). The black symbol indicates 6-dB bandwidth (Bw). Labels above spectral peaks indicate corresponding periods in ka.

5. Discussion

5.1. Potential Factors Influencing the $\Delta\delta^{18}O_{dut\text{-}rub}$ Variations

The $\Delta\delta^{18}O_{dut\text{-}rub}$ can be used as a proxy for the reconstruction of past upper ocean stratification (see section 2.2). However, variations in stratification of the upper water column can occur due to changes in the surface ocean, through changes in sea surface temperature or salinity, and/or in the subsurface layers, owing to vertical displacements of the thermocline depth for example. Therefore, prior to the interpretation of the major $\Delta\delta^{18}O_{dut\text{-}rub}$ variations in our records, it is necessary to evaluate the oceanographic processes that might influence the final $\Delta\delta^{18}O_{dut\text{-}rub}$ recorded at our site.

Core CDH-86 (Nace et al., 2014) provides the nearest Ti/Ca, SST, and $\delta^{18}O_{sw}$ records to our sites (Figure 1b). The Ti/Ca results from core CDH-86 match relatively well our Ti/Ca results from core GL-1248 (Figure S5). Mismatches between both Ti/Ca records only occur during late MIS5 and MIS4 (Figure S5). For late MIS5, the Ti/Ca peak centered at 87 ka in GL-1248 apparently occurs at 90 ka in CDH-86, and this mismatch is probably due to age model uncertainties from both cores. Results from core CDH-86 show an abrupt increase in Ti/Ca at the end of MIS4, possibly linked to HS6, while our results from core GL1248 display high Ti/Ca values during the entire MIS4. Despite this mismatch, our results are in agreement with other studies that indicate increase in precipitation over northeastern Brazil (Wang et al., 2004; Figure S3) and a southward displacement of the ITCZ (Deplazes et al., 2013) during the entire MIS4. The general congruence between the Ti/Ca results from cores CDH-86 and GL-1248 reinforces the notion that both archives record similar climate-related variations in the study area, thus allowing comparisons between records derived from these cores.

Sea surface temperature and $\delta^{18}O_{sw}$ (a proxy for SSS) curves from CDH-86 show similar variations, in which increases in SST and increases (or no significant change) in $\delta^{18}O_{sw}$ occur during the majority of the periods where we observed peaks in $\Delta\delta^{18}O_{dut\text{-}rub}$ values (Figures S6a and S6b). While an increase in SST would decrease the $\delta^{18}O$ of *G. ruber* (white), an increase in $\delta^{18}O_{sw}$ would have the opposite effect. This is a possible explanation for the fact that the amplitude of variations in *G. ruber* (white) $\delta^{18}O$ is not as high as the one in *N. dutertrei* $\delta^{18}O$ during the events of increased stratification (Figures S6c and S6d). Exceptions to this general pattern of SST and $\delta^{18}O_{sw}$ changes are the YD, where a clear reduction in SST and $\delta^{18}O_{sw}$ is observed, and HS4, where a decrease in $\delta^{18}O_{sw}$ can be noticed. Nevertheless, besides the $\Delta\delta^{18}O_{dut\text{-}rub}$ variation during the EH, the responses of the stratification proxy during other periods are predominantly modulated by changes in the $\delta^{18}O$ of *N. dutertrei*. In order to explain our *N. dutertrei* $\delta^{18}O$ record, temperature and $\delta^{18}O_{sw}$ reconstructions at subsurface would be needed, but this type of data is still scarce for this area. To our knowledge, Portilho-Ramos et al. (2017) is the only study that presents a subsurface temperature reconstruction for the last 30 ka in this region, using the Modern Analog Technique applied to planktonic foraminifera assemblages. Their data from core GeoB16206-1 (Figure 1b) indicates a subsurface cooling during HS2, HS1, and the YD, which were associated with a shoaling of the mixed layer (Figure S7a). This is consistent with our observations of increased $\delta^{18}O$ values of *N. dutertrei* during HS1 and the YD (Figure S7a). Hence, the increase in $\delta^{18}O$ of *N. dutertrei* during HS1 and the YD can be explained by a decrease in subsurface temperature, linked to a shoaling of the mixed layer and thermocline depth. In addition, the changes recorded by their $R_{NG/g}$ ratio (proxy for mixed layer depth, Portilho-Ramos et al., 2017) are in agreement with our $\Delta\delta^{18}O_{dut\text{-}rub}$ changes for the LGM, HS1, and the YD. A dissimilarity between both proxies can only be noticed during the EH (Figure S7b). However, it is still important to further assess if the increased stratification was mainly triggered by surface or subsurface changes.

The amplitude of the variations in $\delta^{18}O$ of each species across the periods of major $\Delta\delta^{18}O_{dut\text{-}rub}$ change can serve as an indicator of the prevailing oceanographic processes responsible for the $\Delta\delta^{18}O_{dut\text{-}rub}$ signal. Considering the main periods of increased upper ocean stratification, the amplitude of the variation in

$\delta^{18}O$ of *G. ruber* (white) is only higher than the amplitude of the $\delta^{18}O$ signal of *N. dutertrei* during the EH and HS1 (Figure 6b). Consequently, during these two periods, the variations in SST and $\delta^{18}O_{sw}$ in the surface layer are the dominant factor over the final $\Delta\delta^{18}O_{dut\text{-}rub}$ signature. In the case of HS1, although the amplitude of the variation in $\delta^{18}O$ of *N. dutertrei* is lower compared to the one of *G. ruber* (white), the increase in the $\delta^{18}O$ values of *N. dutertrei* is responsible for approximately one third of the final $\Delta\delta^{18}O_{dut\text{-}rub}$ signal and indicates a shallow thermocline depth during this event. For all the other periods of increased upper ocean stratification, the amplitude of the variation in $\delta^{18}O$ of *N. dutertrei* is larger than the one of *G. ruber* (white), which suggests that changes in the subsurface layer linked to the shoaling of the thermocline depth is the prevailing factor over the recorded $\Delta\delta^{18}O_{dut\text{-}rub}$ signal. Therefore, despite the fact that $\Delta\delta^{18}O_{dut\text{-}rub}$ signal may be dominated by surface ocean changes during certain periods (EH and HS1), in all periods of increased upper ocean stratification, subsurface variations consistent with a shoaling of the thermocline depth are observed. Based on this evidence, it is now possible to explore the mechanisms behind such thermocline depth fluctuations through time in our records.

5.2. Changes in Thermocline Depth in the Western Equatorial Atlantic During Heinrich Stadials

Our $\Delta\delta^{18}O_{dut\text{-}rub}$ record indicates an increase in upper ocean stratification in the western equatorial Atlantic (partly due to a shoaling of the thermocline; see section 5.1) during HS, particularly during HS5a, HS5, and HS1 (Figures 8d and 8h). Our $\Delta\delta^{18}O_{dut\text{-}rub}$ record from GeoB16202-2 agrees with the $R_{N/Gg}$ tracer from core GeoB16206-1 (defined as % *Neogloboquadrina*/ (% *Neogloboquadrina* + % *G. glutinata*, Portilho-Ramos et al., 2017) (Figures 8d and S7), which further supports our interpretation of enhanced upper ocean stratification. Portilho-Ramos et al. (2017) interpret the change in $R_{N/Gg}$ during HS1 as a shallow mixed layer depth, which would allow the presence of thermocline waters closer to the surface. They attribute this shoaling of the mixed layer to changes in the density of the upper water column, caused by enhanced precipitation due to a southward shift of the ITCZ position, which would reduce the efficiency of wind-driven vertical mixing. We propose here that the shoaling of the thermocline depth observed in the western equatorial Atlantic during HS (mostly HS1, HS5, and HS5a; Figure 8) results from the reduced SEC transport of warm waters due to a weakening of SE trades winds, similar to what occurs during modern boreal winter (see section 2.1 and Figure 2), on top of the mechanism proposed by Portilho-Ramos et al. (2017). Indeed, even though different triggers and mechanisms are proposed here and in Portilho-Ramos et al. (2017) to explain the observed changes in upper ocean stratification, we do not discard the possibility that both mechanisms could be acting synergistically to increase upper ocean stratification in this region during HS.

The agreement between these different proxies ($\Delta\delta^{18}O_{dut\text{-}rub}$ and $R_{N/Gg}$) only supports the notion that upper ocean stratification changed locally (offshore northeastern Brazil) during HS. In order to verify if the changes in thermocline depth occurred at, at least, the regional scale, we compared our results with other available records from the western equatorial Atlantic and from the eastern Atlantic that have enough resolution to resolve millennial-scale events (Figure 8). In the western equatorial Atlantic, we compare our results with planktonic foraminifera assemblages from sediment core M35003-4 (Hüls & Zahn, 2000) located north of the equator. We calculated downcore changes in the $R_{N/Gg}$ ratio (Portilho-Ramos et al., 2017) from faunal assemblages of core M35003-4, to allow for a more direct comparison of variations in upper ocean stratification. Increases in our $\Delta\delta^{18}O_{dut\text{-}rub}$ values match decreases in the $R_{N/Gg}$ values from core M35003-4 during several HS (Figure 8), indicating antiphased stratification changes to the north and south of the equator in the western equatorial Atlantic during these events. We propose that this antiphase behavior is a response to hemispherically asymmetric trade wind changes during HS, which is supported by further proxy data, as discussed below.

There is multiple evidence for weakened (strengthened) SE (NE) trade winds in the Atlantic during HS. As pointed out by McGee et al. (2018), the highest-quality records documenting the strength of SE and NE trade winds are located in the southeastern and northeastern Atlantic, respectively. In the subtropical southeastern Atlantic, well-dated alkenone-derived SST records support the occurrence of weak SE trade winds during HS1 (Kim et al., 2003), by showing a weak upwelling south of the Angola-Benguela Front and less tropical warm-water transport toward the area north of this oceanic front. Other proxy records from the SE Atlantic endorse the scenario of a weakening of the SE trades during HS (Figure 8). Decreases in the abundance of a cold-water foraminifera species (e.g., *Neogloboquadrina pachyderma* sinistral) in the SE Atlantic during HS1, HS5, and HS5a (Little et al., 1997) suggest a weak Benguela upwelling, which is linked to weakened SE trades winds

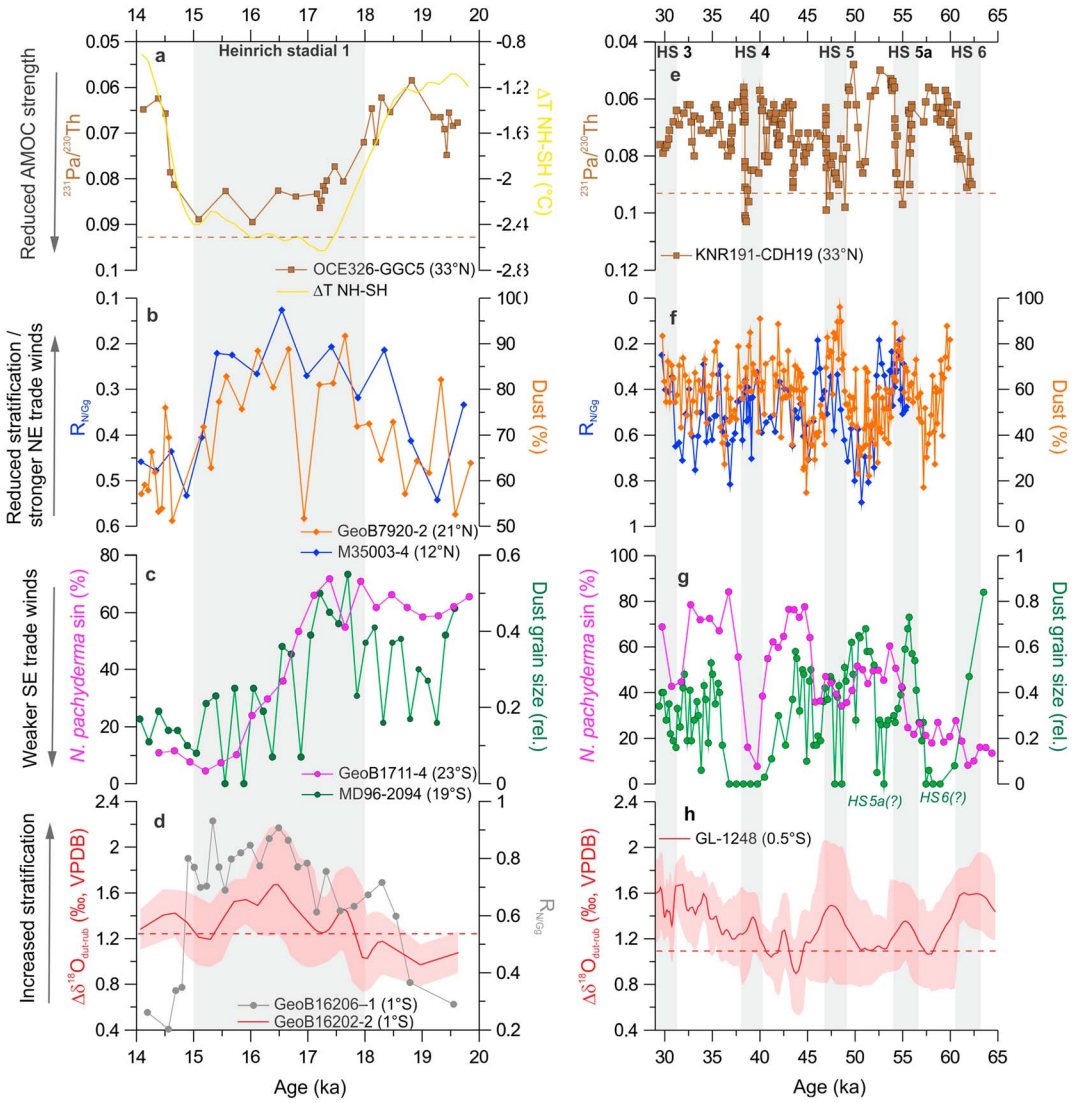

Figure 8. Upper ocean stratification in the western equatorial Atlantic during Heinrich stadials compared to other proxies. (a) $^{231}Pa/^{230}Th$ records from core OCE326-GGC5 from the Bermuda rise (McManus et al., 2004; brown line and squares) and reconstruction of hemispheric surface temperature difference (Shakun et al., 2012; yellow line). The brown dotted line represents the $^{231}Pa/^{230}Th$ production ratio of 0.093, which indicates sluggish or absent overturning circulation. (b) Stratification proxy from the western tropical North Atlantic and a dust record from the eastern tropical North Atlantic. The $R_{N/Gg}$ ratio (%*Neogloboquadrina*/(%*Neogloboquadrina* + %*G. glutinata*) from core M35003-4 (Hüls & Zahn, 2000; Portilho-Ramos et al., 2017; blue line and diamonds) in the western tropical North Atlantic. Relative percentage of dust from core GeoB7920-2 (Collins et al., 2013; orange line and diamonds) in the eastern tropical North Atlantic. (c) Proxies from the subtropical South Atlantic near the Benguela upwelling system (Figure 1b) linked to southeast trade wind intensity. Relative abundance of *Neogloboquadrina pachyderma* (sinistral) from core GeoB1711-4 (Little et al., 1997; pink line and circles). Relative abundance of coarse-grained dust to total windblown dust from core MD96-2094 (Stuut et al., 2002; green line and circles). (d) Proxies for stratification in the western equatorial Atlantic. The $R_{N/Gg}$ ratio (%*Neogloboquadrina*/(%*Neogloboquadrina* + %*G. glutinata*) from core GeoB16206-1 (Portilho-Ramos et al., 2017; gray line and circles) and the Monte Carlo ensemble $\Delta\delta^{18}O_{dut\text{-}rub}$ mean values from core GeoB16202-2 (this study; red line). Red shading indicates the 95% confidence envelope including age and analytical uncertainties. The red dotted line represents the $\Delta\delta^{18}O_{dut\text{-}rub}$ core top value from GeoB16202-2. The gray bar marks the time interval of Heinrich stadial 1 (18–15 ka). (e) $^{231}Pa/^{230}Th$ records from core KNR191-CDH19 also from the Bermuda rise (Henry et al., 2016; brown line and squares). The brown dotted line represents the $^{231}Pa/^{230}Th$ production ratio of 0.093. (e) Same records as in (b). (f) Same records as in (c). (g) The Monte Carlo ensemble $\Delta\delta^{18}O_{dut\text{-}rub}$ mean values from core GL-1248 (red line), with the red 95% confidence envelope (red shading). The red dotted line represents the $\Delta\delta^{18}O_{dut\text{-}rub}$ core top value from GL-1248. Gray bars highlight the Heinrich stadials (HS3, HS4, HS5, HS5a, and HS6). Note that the published records presented here are shown on their original chronologies.

(Figures 8c and 8g). Moreover, reductions in dust grain size in SE Atlantic sediments during HS1 and HS5 (Stuut et al., 2002) reflect a reduced wind transport of coarse-grained dust from the continent, thus indicating weakened SE trades (Figures 8c and 8g). In contrast, the dust record from Stuut et al. (2002) seems to suggest an intensification of winds during HS5a (Figure 8g). However, very low values of grain

size observed around 53 ka could highlight a delayed response of this proxy during HS5a, or the result of age model uncertainties. Nevertheless, the trade wind proxies from the Benguela upwelling system generally show good agreement and suggest weakened SE trades winds during HS1, HS5, and HS5a (Figures 8c and 8g). In the tropical northeastern Atlantic, several records indicate increases in windblown dust transport during HS, which reflect increases in NE trade winds (McGee et al., 2018; Mulitza et al., 2008). Dust records from the work of Collins et al. (2013) provide information regarding wind strength for the last 60 ka and show increases in NE trade winds during several HS. In addition, the increases in the strength of NE trade winds, revealed from the dust record of core GeoB7920-2 (Collins et al., 2013), match considerably well the increases in mixed layer depth at the western equatorial North Atlantic, represented by the $R_{N/Gg}$ variations from core M35003-4 (Hüls & Zahn, 2000), during several HS (Figures 8b and 8f). This observation provides further support to the assumption that the antiphase behavior between upper ocean stratification north and south of the western equatorial Atlantic is linked to the asymmetric response of the trade winds during HS. The weakening (strengthening) of SE (NE) trade winds during HS is supported by angular momentum constrains and model results (McGee et al., 2018). This response occurs due to a cooling of the Northern Hemisphere compared to the Southern Hemisphere, where a southward shift of the ITCZ position is followed by a weakening (strengthening) of the Southern (Northern) Hemisphere Hadley cell and associated trade winds (Chiang & Friedman, 2012; McGee et al., 2018). Such adjustment of the ITCZ position resulted from the enhanced cross-equatorial temperature gradient (with a widespread South Atlantic warming, e.g., Shakun et al., 2012) and the reduced northward ocean heat transport (Frierson et al., 2013) that were caused by the slowdown of the AMOC during HS (McManus et al., 2004; Stocker, 1998).

We now use the analogy of the modern boreal winter situation to discuss how weak SE (strong NE) trade winds could be responsible for a shoaling (deepening) of the thermocline and increased (decreased) upper ocean stratification recorded in the western equatorial South (tropical North) Atlantic, as for a relaxation of the east-west equatorial thermocline tilt, during HS (Figure 8). In the western equatorial South Atlantic, since the intensity of the SEC and the NBC transports is modulated by the SE trade winds (Johns et al., 1998; Stramma et al., 1995), the observed reductions in the strength of the SE trade winds during HS probably influenced the transport of heat from the South Atlantic into the North Atlantic. Under modern conditions, when SE trade winds are weak, a reduction in the SEC and in the NBC transport can be observed (see section 2.1). Thus, during HS, a decrease in the transport of the SEC, particularly the central branch (cSEC), probably promoted a reduction in the transport of warm waters from east to west, producing a shoaling of the thermocline in the western equatorial South Atlantic (Figure 8). In the western tropical North Atlantic, the highest westward transport of the Caribbean Current occurs during boreal winter, when the NE trade winds are at their maximum strength (Murphy et al., 1999; Vink et al., 2001). During this period, surface waters pile up along the northern boundary of the Caribbean Sea due to the increase in the wind stress of NE trades (Kinder et al., 1985; Vink et al., 2001). The stacking of surface waters probably increased during HS, in response to increased NE trade winds, and caused a deepening of the thermocline in the western tropical North Atlantic (Figure 8). It is also noteworthy that the weak tropical easterlies during HS would also decrease the divergence in the eastern equatorial Atlantic and produce a shoaling of the thermocline in this region. Because the eastern equatorial Atlantic divergence and western Atlantic thermocline depth are both connected to changes in the intensity of the SE trade winds (Hastenrath & Merle, 1987), the aforementioned process probably promoted a relaxation of the east-west thermocline tilt. This is in agreement with the findings from McIntyre and Molfino (1996), showing decreases in wind-driven divergence in the eastern equatorial Atlantic during several HS, and with our results, which confirm a shallow thermocline in the west for the same events. Spectral analysis provides additional support to the notion that both east (McIntyre & Molfino, 1996) and west (this study) records are linked through a similar forcing or mechanism, since both studies present similar centennial- to millennial-scale periodicities (~0.8 and 7.4 kyr). The presence of a 7- to 8-kyr cycle further supports the idea of a link between low-latitude climate modulated by precessional forcing and the rather regular timing of HS (HS6 to HS1), described by previous studies (De Winter et al., 2014; Heinrich, 1988; McIntyre & Molfino, 1996). These observations endorse the idea of a broad-scale change in thermocline depth in the equatorial Atlantic during HS. Moreover, the southward migration of the ITCZ during HS should also promote a northward displacement of the SEC bifurcation, which also contributes to a reduction in the NBC transport (Rodrigues et al., 2007). Thus, during HS, the cross-equatorial transport of warm surface waters to the North Atlantic probably decreased following the reductions in the intensity of

these ocean currents triggered by the proposed mechanisms. This is also in line with the observations in the western tropical Atlantic from Weldeab et al. (2006), indicating a less vigorous NBC and a reduced transport of warm surface waters to the North Atlantic during periods of decreased AMOC strength. Therefore, such alterations in the vertical structure of the water column and in the wind-driven ocean circulation in the equatorial Atlantic might have contributed as an additional climatic perturbation to the already reduced AMOC strength.

Interestingly, during HS4 and HS6, periods of marked reductions in the AMOC strength (Henry et al., 2016; Figure 8e) and SE trade wind intensity (Little et al., 1997; Stuut et al., 2002; Figure 8g), our $\Delta\delta^{18}O_{dut\text{-}rub}$ record from GL-1248 only indicates a minor increase in upper ocean stratification (Figure 8h). In our $\Delta\delta^{18}O_{dut\text{-}rub}$ record, the weak responses during HS4 and HS6 seem to be part of long-term trends. For HS4, the response is part of a trend toward increased upper ocean stratification ranging from 45 to 30 ka, while for HS6 it is part of an overall increase in $\Delta\delta^{18}O_{dut\text{-}rub}$ during MIS4 (Figure 8h). These long-term trends in the $\Delta\delta^{18}O_{dut\text{-}rub}$ values are mainly driven by variations in the $\delta^{18}O$ of *N. dutertrei* (Figure 6), indicating a change in the thermocline depth. In addition, the shallow thermocline observed for MIS4 at our site seems to correspond with a deep thermocline in the eastern equatorial Atlantic, as indicated by the relative abundances of *Florisphaera profunda* from cores RC2402 and RC2417 (McIntyre & Molfino, 1996). Such long-term trends in our record are probably related to orbital-scale variability (section 5.3), which may mask the millennial-scale variations at our core site during late MIS3 and MIS4.

5.3. Upper Ocean Stratification Changes in the Western Equatorial Atlantic Linked to Variations in Trade Wind Zonality

Previous studies support the idea of the strength of SE trade winds acting as the main driver of changes in the thermocline depth on glacial-interglacial timescales in the western equatorial Atlantic. Analyzing planktonic foraminiferal assemblages from cores GeoB2204-2 and GeoB1523-1 (Figure 1b), Wolff et al. (1999) suggested that during glacials, steep meridional temperature gradients over the Southern Hemisphere led to strong SE trade winds, which caused a deepening of the thermocline in the western tropical Atlantic. Using the relative abundances of *Florisphaera profunda* from Kinkel et al. (2000) and the oxygen isotopic difference ($\Delta\delta^{18}O$) between *T. sacculifer* and *Globorotalia tumida* as proxies for upper ocean stratification, Rühlemann et al. (2001) also show a deepening of the thermocline during the cold stages of MIS5 in core GeoB1523-1, supporting the mechanism described by Wolff et al. (1999). Trade-wind related proxies from the subtropical SE Atlantic (Figure 9a) also suggest strong SE trade winds during glacials and cold substages of the last 130 ka. Based on these findings, we expected to observe at our core site a deepening of the thermocline during these cold periods of enhanced SE trade winds. Contrary to our expectations, our new $\Delta\delta^{18}O_{dut\text{-}rub}$ records show that a shallow thermocline occurred in the western equatorial Atlantic during MIS5d, MIS5b, MIS4, and late MIS3 (Figure 9b). This result indicates that in contrast to glacial millennial-scale events, the strength of the SE trade winds was not the main driver of upper ocean stratification changes in the western tropical Atlantic during these periods and that other mechanisms need to be considered.

The $\Delta\delta^{18}O_{dut\text{-}rub}$ variations in our records appear to be coupled with low latitude Northern Hemisphere summer insolation changes modulated by the precessional component (Figure 9b). This is in line with the idea that the tropical trade wind system responds to insolation changes, which in the past were largely modulated by precessional variations (McIntyre et al., 1989; McIntyre & Molfino, 1996; Molfino & McIntyre, 1990; Schneider et al., 1995). Spectral analysis performed on our $\Delta\delta^{18}O_{dut\text{-}rub}$ records (Figure 7) shows significant periodicities in the 19- to 23-kyr frequency band, which supports the direct response of upper ocean stratification to precession. Wolff et al. (1999) did not observe precessional-related cycles in their records, probably due to the locations of their cores, which were more influenced by the NECC (GeoB1523-1) and by the southern branch of the SEC (GeoB2204-2). Because our core sites receive surface waters from the eastern equatorial Atlantic via the central branch of the SEC, they are more suited to capture past variations in east-to-west thermocline tilt, which are closely linked to the dynamics of the SE trade winds (Hastenrath & Merle, 1987) modulated by precession (McIntyre et al., 1989; McIntyre & Molfino, 1996; Molfino & McIntyre, 1990).

Our $\Delta\delta^{18}O_{dut\text{-}rub}$ records show increased stratification during periods of Northern Hemisphere summer insolation maxima (Figure 9b). These periods are also intervals of minimal SE trades zonality, as suggested by previous studies (McIntyre et al., 1989; Molfino & McIntyre, 1990; Schneider et al., 1995). The zonal component of

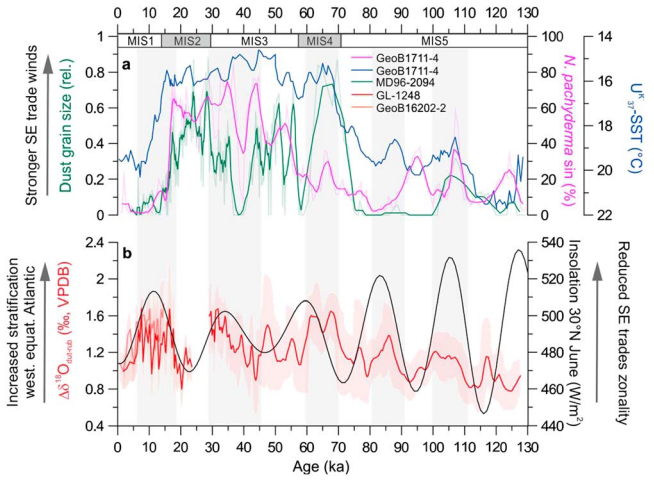

Figure 9. Upper ocean stratification in the western equatorial Atlantic compared to trade wind strength and zonality for the last 130 ka. (a) Proxies from the subtropical South Atlantic near the Benguela upwelling system (Figure 1b) linked to southeast trade wind intensity. Relative abundance of *N. pachyderma* (sinistral) from core GeoB1711-4 (Little et al., 1997; pink line) with a 5-point running average (thick pink line). Relative abundance of coarse-grained dust to total windblown dust from core MD96-2094 (Stuut et al., 2002; green line) with a 5-point running average (thick green line). Alkenone-based sea surface temperatures from core GeoB1711-4 (Kirst et al., 1999; blue line). (b) Our Monte Carlo ensemble $\Delta\delta^{18}O_{dut\text{-}rub}$ mean values from cores GeoB16202-2 (red line) and GL-1248 (red line for the lower part and light red line for the upper part of the record). Shadings with the same color code indicate the 95% confidence envelope including age and analytical uncertainties. Mid-June 30°N insolation (solid gray line) are displayed (Berger & Loutre, 1991). Marine isotope stages (MIS) are highlighted below the upper *x*-axis. Gray bars highlight key periods of increased stratification on our $\Delta\delta^{18}O_{dut\text{-}rub}$ records (GL-1248 and GeoB16202-2) and increased mid-June 30°N insolation.

the SE trades weakens or strengthens depending on precession-related changes in Northern Hemisphere summer insolation and on the intensity of the monsoon over North Africa (Schneider et al., 1995). When perihelion was centered on boreal summer, North African monsoon intensified and weakened the zonal component of the tropical easterlies (Bassinot et al., 1997; McIntyre et al., 1989; Molfino & McIntyre, 1990). Less zonal SE trades would then reduce the westward transport of warm waters via the central branch of the SEC and induce a shallow thermocline in the western equatorial Atlantic, as observed during MIS5d, MIS5b, MIS4, and late MIS3 (Figure 9b).

Low-latitude insolation changes at semiprecessional timescales (Berger et al., 2006; McIntyre & Molfino, 1996) may also have modulated the intensity of the SE trade winds, consequently influencing upper ocean stratification at our sites. Over one precessional cycle, there are two moments where perihelion is coincident with the solstice in Northern Hemisphere summer (Berger et al., 2006; McIntyre & Molfino, 1996), and thus, two intervals of minimum zonality of the tropical easterlies may have occurred. Although in the tropics the dominant forcing would still be the primary precessional components (19–23 kyr), this effect would produce harmonic periods with values of 11 and 9.5 kyr (McIntyre & Molfino, 1996). In the eastern equatorial Atlantic, McIntyre and Molfino (1996) observed periodicities centered on 7.6 to 8.4 kyr on the relative abundance of the coccolithophore *Florisphaera profunda* of several cores and concluded that variations in the zonal wind-driven divergence were produced by a semiprecessional component. The spectral analysis performed on our $\Delta\delta^{18}O_{dut\text{-}rub}$ records (Figure 7) also show the presence of periodicities centered at 7.4 kyr. This result indicates that the zonal intensity of the SE trade winds modulated by a semiprecessional component was also an important driver of stratification changes in the western equatorial Atlantic. These findings reinforce the close connection between the eastern and western equatorial Atlantic regarding upper ocean stratification changes related to SE trade winds zonality (Hastenrath & Merle, 1987). These results also support the idea of McIntyre and Molfino (1996) that advection of low-latitude warm surface waters to the high-latitude North Atlantic is influenced by variations in the zonality of the tropical easterlies.

Finally, our $\Delta\delta^{18}O_{dut\text{-}rub}$ record from GL-1248 reveals MIS4 as an interesting period in the western equatorial Atlantic. During MIS4, high boreal summer insolation is responsible for less zonal SE trade winds and for the shallow thermocline indicated by the high $\Delta\delta^{18}O_{dut\text{-}rub}$ values. Although the evolution of $\Delta\delta^{18}O_{dut\text{-}rub}$ from core GL-1248 does not exactly follow insolation changes during MIS4 (Figure 9b), a deepening of the thermocline is observed in records located in the eastern equatorial Atlantic for the same period (McIntyre & Molfino, 1996). This observation gives further support to the idea of coupled east-west thermocline tilt changes. In addition, we propose here that the mechanism described by Portilho-Ramos et al. (2017) was probably operating during MIS4. The shallow thermocline during early MIS4 would thus be related to changes in the density of the upper water column, caused by enhanced direct precipitation over the ocean due to a southward shift of the ITCZ position. A southward position of the ITCZ during the entire MIS4 is supported by speleothem records (Wang et al., 2004) from NE Brazil and reflectance data from Cariaco Basin (Deplazes et al., 2013). Such an ITCZ shift then probably promoted a decrease in the NBC transport due to a northward displacement of the SEC bifurcation (Rodrigues et al., 2007). Thus, the less zonal tropical easterlies did not favor the transport of warm waters via the central branch of the SEC to the western equatorial Atlantic, consequently reducing the cross-equatorial transport of warm waters. Particularly, such a reduction in the transport of surface warm waters to higher latitudes during MIS4, possibly contributed to the glacial descent in the midlatitudes and high latitudes described by Barker and Diz (2014), and led to the storage of warm waters in the low latitudes of the western tropical Atlantic as suggested by Santos et al. (2017). These observations emphasize the importance of climatic mechanisms linked to the wind-driven ocean circulation at low latitudes for

determining the density structure and the pathway of the waters that will enter the North Atlantic and contribute to the upper-limb of the AMOC.

6. Conclusions

Our new $\Delta\delta^{18}O_{dut\text{-}rub}$ records document changes in thermocline depth in the western equatorial Atlantic on both millennial and orbital timescales since the LIG. On millennial timescales, the $\Delta\delta^{18}O_{dut\text{-}rub}$ record suggests enhanced upper ocean stratification during several HS (i.e., HS1, HS5, and HS5a), partly due to a shoaling of the thermocline depth. The shoaling of the thermocline was linked to a weakening of the SE trade winds due to a widespread warming of the South Atlantic during periods of reduced AMOC strength. The $\Delta\delta^{18}O_{dut\text{-}rub}$ signal during other HS (i.e., HS3, HS4, and HS6) is likely masked by long-term trends. On longer timescales, changes in thermocline depth at our study area cannot be explained by the changing strength of the SE trades, and we propose that variations in SE trade winds zonality play an important role. During periods of low latitude Northern Hemisphere summer insolation maxima, the SE trade winds were less zonal, promoting a relaxation of the thermocline depth in the western equatorial Atlantic. This process is particularly important to explain the shoaling of the thermocline during the late MIS3, MIS4, and the cold substages of MIS5. During MIS4, the variations in upper ocean stratification do not exactly follow insolation changes, and we proposed that changes in the density of the upper water column, caused by enhanced direct precipitation over the ocean due to a southward shift of the ITCZ position acted as an additional mechanism. The observed past changes in water column structure and wind-driven circulation probably caused a reduction in the transport of warm surface waters to high latitudes of the North Atlantic during HS, as well as during MIS4.

Acknowledgments

This research used data acquired at the XRF Core Scanner Lab at the MARUM – Center for Marine Environmental Sciences, University of Bremen, Germany. We thank R. Kowsman (CENPES/Petrobras) and Petrobras Core Repository staff (Macaé/Petrobras) for providing sediment core GL-1248. This study was supported by CAPES-ASPECTO project (Grant 88887.091731/2014-01). A.L.S. Albuquerque is a CNPq (National Council for the Development of Science and Technology, Brazil) senior researcher (Grant 302521/2017-8). CNPq also financially supported Igor M. Venancio with a scholarship from the CsF ("Ciencia sem Fronteiras") project (Grant 248819/2013-5). CAPES currently financially supports Igor M. Venancio with a scholarship (Grant 88887.156152/2017-00 and 88881.161151/2017-01). This work was also funded through the DFG Research Center/Cluster of Excellence "The Ocean in the Earth System" and by the Helmholtz Climate Initiative REKLIM. This is LSCE publication number 6541. C. M. Chiessi acknowledges the financial support from FAPESP (Grant 2012/17517-3), CAPES (Grants 1976/2014 and 564/2015), and CNPq (Grants 302607/2016-1 and 422255/2016-5). The data reported in this paper are available in Data Set S1 and are archived in Pangaea (https://doi.pangaea.de/10.1594/PANGAEA.895049). We thank two anonymous reviewers for their constructive comments that greatly improved this manuscript.

References

Arbuszewski, J., DeMenocal, P., Kaplan, A., & Farmer, E. C. (2010). On the fidelity of shell-derived δ^{18}Oseawater estimates. *Earth and Planetary Science Letters*, *300*(3–4), 185–196. http://doi.org/10.1016/j.epsl.2010.10.035

Arz, H. W., Pätzold, J., & Wefer, G. (1998). Correlated millennial-scale changes in surface hydrography and terrigenous sediment yield inferred from last-glacial marine deposits off northeastern Brazil. *Quaternary Research*, *50*(02), 157–166. http://doi.org/10.1006/qres.1998.1992

Barker, S., & Diz, P. (2014). Timing of the descent into the last Ice Age determined by the bipolar seesaw. *Paleoceanography*, *29*, 489–507. https://doi.org/10.1002/2014PA002623

Bassinot, F. C., Beaufort, L., Vincent, E., & Labeyrie, L. (1997). Changes in the dynamics of western equatorial Atlantic surface currents and biogenic productivity at the mid-Pleistocene revolution (930 ka). *Proceedings of the Ocean Drilling Program*, *154*, 573. http://doi.org/10.2973/odp.proc.sr.154.108.1997

Baumgartner, M., Kindler, P., Eicher, O., Floch, G., Schilt, A., Schwander, J., et al. (2014). NGRIP CH4 concentration from 120 to 10 kyr before present and its relation to a δ15N temperature reconstruction from the same ice core. *Climate of the Past*, *10*(2), 903–920. http://doi.org/10.5194/cp-10-903-2014

Bemis, B. E., Spero, H. J., Bijma, J., & Lea, D. W. (1998). Reevaluation of the oxygen isotopic composition of planktonic foraminifera: Experimental results and revised paleotemperature equations. *Paleoceanography*, *13*(2), 150–160. https://doi.org/10.1029/98PA00070

Berger, A., & Loutre, M. F. (1991). Insolation values for the climate of the last 10 million years. *Quaternary Science Reviews*, *10*(4), 297–317. http://doi.org/10.1016/0277-3791(91)90033Q

Berger, A. L., Loutre, M. F., & Mélice, J. L. (2006). Equatorial insolation: From precession harmonics to eccentricity frequencies. *Climate of the Past*, *2*(4), 519–533. http://doi.org/10.5194/cpd-2-519-2006

Blaauw, M. (2010). Methods and code for "classical" age-modelling of radiocarbon sequences. *Quaternary Geochronology*, *5*(5), 512–518. http://doi.org/10.1016/j.quageo.2010.01.002

Blaauw, M., & Christen, J. A. (2011). Flexible paleoclimate age-depth models using an autoregressive gamma process. *Bayesian Analysis*, *6*(3), 457–474. https://doi.org/10.1214/11-BA618

Bouvier-Soumagnac, Y., & Duplessy, J. C. (1985). Carbon and oxygen isotopic composition of planktonic foraminifera from laboratory cultures, plankton tows, and recent sediments: Implications for the reconstruction of paleoclimatic conditions and the global carbon cycle. *Journal of Foraminiferal Research*, *15*(4), 302–320. https://doi.org/10.2113/gsjfr.15.4.302

Breitenbach, S. F. M., Rehfeld, K., Goswami, B., Baldini, J. U. L., Ridley, H. E., Kennett, D. J., et al. (2012). Constructing proxy records from age models (COPRA). *Climate of the Past*, *8*(5), 1765–1779. http://doi.org/10.5194/cp-8-1765-2012

Chappellaz, J., Bluniert, T., Raynaud, D., Barnola, J. M., Schwander, J., & Stauffert, B. (1993). Synchronous changes in atmospheric CH_4 and Greenland climate between 40 and 8 kyr BP. *Nature*, *366*(6454), 443–445. http://doi.org/10.1038/366443a0

Chiang, J. C. H., & Friedman, A. R. (2012). Extratropical cooling, interhemispheric thermal gradients, and Tropical Climate Change. *Annual Review of Earth and Planetary Sciences*, *40*(1), 383–412. http://doi.org/10.1146/annurev-earth-042711-105545

Cléroux, C., Demenocal, P., Arbuszewski, J., & Linsley, B. (2013). Reconstructing the upper water column thermal structure in the Atlantic Ocean. *Paleoceanography*, *28*, 503–516. https://doi.org/10.1002/palo.20050

Collins, J. A., Govin, A., Mulitza, S., Heslop, D., Zabel, M., Hartmann, J., et al. (2013). Abrupt shifts of the Sahara-Sahel boundary during Heinrich stadials. *Climate of the Past*, *9*(3), 1181–1191. http://doi.org/10.5194/cp-9-1181-2013

De Winter, N. J., Zeeden, C., & Hilgen, F. J. (2014). Low-latitude climate variability in the Heinrich frequency band of the Late Cretaceous greenhouse world. *Climate of the Past*, *10*(3), 1001–1015. http://doi.org/10.5194/cp-10-1001-2014

Deplazes, G., Lückge, A., Peterson, L. C., Timmermann, A., Hamann, Y., Hughen, K. A., et al. (2013). Links between tropical rainfall and North Atlantic climate during the last glacial period. *Nature Geoscience*, *6*(3), 213–217. http://doi.org/10.1038/ngeo1712

Farmer, E. C., Kaplan, A., de Menocal, P. B., & Lynch-Stieglitz, J. (2007). Corroborating ecological depth preferences of planktonic foraminifera in the tropical Atlantic with the stable oxygen isotope ratios of core top specimens. *Paleoceanography*, *22*, PA3205. https://doi.org/10.1029/2006PA001361

Frierson, D. M. W., Hwang, Y. T., Fučkar, N. S., Seager, R., Kang, S. M., Donohoe, A., et al. (2013). Contribution of ocean overturning circulation to tropical rainfall peak in the Northern Hemisphere. *Nature Geoscience*, *6*(11), 940–944. http://doi.org/10.1038/ngeo1987

Goni, G. J., & Johns, W. E. (2001). A census of North Brazil current rings observed from TOPEX/POSEIDON altimetry: 1992–1998. *Geophysical Research Letters*, *28*(1), 1–4. https://doi.org/10.1029/2000GL011717

Govin, A., Capron, E., Tzedakis, P. C., Verheyden, S., Ghaleb, B., Hillaire-Marcel, C., et al. (2015). Sequence of events from the onset to the demise of the Last Interglacial: Evaluating strengths and limitations of chronologies used in climatic archives. *Quaternary Science Reviews*, *129*, 1–36. http://doi.org/10.1016/j.quascirev.2015.09.018

Govin, A., Holzwarth, U., Heslop, D., Ford Keeling, L., Zabel, M., Mulitza, S., et al. (2012). Distribution of major elements in Atlantic surface sediments (36°N-49°S): Imprint of terrigenous input and continental weathering. *Geochemistry, Geophysics, Geosystems*, *13*, Q01013. https://doi.org/10.1029/2011GC003785

Hammer, Ø., Harper, D. A. T., & Ryan, P. D. (2001). PAST: Paleontological statistics software package for education and data analysis. *Palaeontologia Electronica*, *76*(4), 1–9. http://doi.org/10.1016/j.bcp.2008.05.025

Hastenrath, S. (2012). Exploring the climate problems of Brazil's Nordeste: A review. *Climatic Change*. http://doi.org/10.1007/s10584-011-0227-1, *112*(2), 243–251.

Hastenrath, S., & Merle, J. (1987). Annual cycle of subsurface thermal structure in the tropical Atlantic Ocean. *Journal of Physical Oceanography*, *17*(9), 1518–1538. https://doi.org/10.1175/1520-0485(1987)017<1518:ACOSTS>2.0.CO;2

Heinrich, H. (1988). Origin and consequences of cyclic ice rafting in the Northeast Atlantic Ocean during the past 130,000 years. *Quaternary Research*, *29*(02), 142–152. http://doi.org/10.1016/0033-5894(88)90057-9

Henry, L. G., McManus, J. F., Curry, W. B., Roberts, N. L., Piotrowski, A. M., & Keigwin, L. D. (2016). North Atlantic Ocean circulation and abrupt climate change during the last glaciation. *Science*, *353*(6298), 470–474. http://doi.org/10.1126/science.aaf5529

Huber, C., Leuenberger, M., Spahni, R., Flückiger, J., Schwander, J., Stocker, T. F., et al. (2006). Isotope calibrated Greenland temperature record over marine isotope stage 3 and its relation to CH4. *Earth and Planetary Science Letters*, *243*(3-4), 504–519. https://doi.org/10.1016/j.epsl.2006.01.002

Hüls, M., & Zahn, R. (2000). Millennial-scale sea surface temperature variability in the western tropical North Atlantic from planktonic foraminiferal census counts. *Paleoceanography*, *15*(6), 659–678. http://doi.org/10.1029/1999PA000462

Huppertz, N. (2014). Variability of surface water stratification offshore Brazil over the past 25ka. Master's Thesis, University of Bremen, pp. 30.

Hut, G. (1987). Stable isotope reference samples for geochemical and hydrological investigations. Report of Consultant's Group Meeting. *International Atomic Energy Agency* (p. 42). Vienna, Austria.

Jaeschke, A., Rühlemann, C., Arz, H., Heil, G., & Lohmann, G. (2007). Coupling of millennial-scale changes in sea surface temperature and precipitation off northeastern Brazil with high-latitude climate shifts during the last glacial period. *Paleoceanography*, *22*, PA4206. https://doi.org/10.1029/2006PA001391

Johns, W. E., Lee, T. N., Beardsley, R. C., Candela, J., Limeburner, R., & Castro, B. (1998). Annual cycle and variability of the North Brazil Current. *Journal of Physical Oceanography*, *28*(1), 103–128. https://doi.org/10.1175/1520-0485(1998)028<0103:ACAVOT>2.0.CO;2

Kim, J. H., Schneider, R. R., Mulitza, S., & Müller, P. J. (2003). Reconstruction of SE trade-wind intensity based on sea-surface temperature gradients in the Southeast Atlantic over the last 25 kyr. *Geophysical Research Letters*, *30*(22), 2144. http://doi.org/10.1029/2003GL017557

Kinder, T. H., Heburn, G. W., & Green, A. W. (1985). Some aspects of the Caribbean circulation. *Marine Geology*, *68*(1–4), 25–52. http://doi.org/10.1016/0025-3227(85)90004-0

Kinkel, H., Baumann, K. H., & Cepek, M. (2000). Coccolithophores in the equatorial Atlantic Ocean: Response to seasonal and late Quaternary surface water variability. *Marine Micropaleontology*, *39*, 87–112. https://doi.org/10.1016/S0377-8398(00)00016-5

Kirst, G. J., Schneider, R. R., Müller, P. J., Von Storch, I., & Wefer, G. (1999). Late Quaternary temperature variability in the Benguela current system derived from Alkenones. *Quaternary Research*, *52*(01), 92–103. http://doi.org/10.1006/qres.1999.2040

Little, M. G., Schneider, R. R., Kroon, D., Price, B., Summerhayes, C. P., & Segl, M. (1997). Trade wind forcing of upwelling, seasonally, and Heinrich events as a response to sub-Milankovitch climate variability. *Paleoceanography*, *12*(4), 568–576. https://doi.org/10.1029/97PA00823

Locarnini, R. A., Mishonov, A. V., Antonov, J. I., Boyer, T. P., Garcia, H. E., Baranova, O. K., et al. (2013). World Ocean Atlas 2013, Volume 1: Temperature. In S. Levitus & A. Mishonov (Eds.), *NOAA Atlas NESDIS 73* (p. 40). Silver Spring, MD: U.S. Government Printing Office.

Loulergue, L., Schilt, A., Spahni, R., Masson-Delmotte, V., Blunier, T., Lemieux, B., et al. (2008). Orbital and millennial-scale features of atmospheric CH_4 over the past 800,000 years. *Nature*, *453*(7193), 383–386. http://doi.org/10.1038/nature06950

Marengo, J. A., Druyan, L. M., & Hastenrath, S. (1993). Observational and modelling studies of Amazonia interannual climate variability. *Climatic Change*, *23*(3), 267–286. http://doi.org/10.1007/BF01091619

McGee, D., Moreno-Chamarro, E., Green, B., Marshall, J., Galbraith, E., & Bradtmiller, L. (2018). Hemispherically asymmetric trade wind changes as signatures of past ITCZ shifts. *Quaternary Science Reviews*, *180*, 214–228. http://doi.org/10.1016/j.quascirev.2017.11.020

McIntyre, A., & Molfino, B. (1996). Forcing of Atlantic equatorial and subpolar millennial cycles by precession. *Science*, *274*(5294), 1867–1870. https://doi.org/10.1126/science.274.5294.1867

McIntyre, A., Ruddiman, W. F., Karlin, K., & Mix, A. C. (1989). Surface water response of the equatorial Atlantic Ocean to orbital forcing. *Paleoceanography*, *4*(1), 19–55. https://doi.org/10.1029/PA004i001p00019

McManus, J. F., Francois, R., Gherardl, J. M., Kelgwin, L., & Drown-Leger, S. (2004). Collapse and rapid resumption of Atlantic meridional circulation linked to deglacial climate changes. *Nature*, *428*(6985), 834–837. http://doi.org/10.1038/nature02494

Molfino, B., & McIntyre, A. (1990). Precessional forcing of nutricline dynamics in the equatorial Atlantic. *Science (New York, N.Y.)*, *249*(4970), 766–769. http://doi.org/10.1126/science.249.4970.766

Mulitza, S., Boltovskoy, D., Donner, B., Meggers, H., Paul, A., & Wefer, G. (2003). Temperature: $\delta^{18}O$ relationships of planktonic foraminifera collected from surface waters. *Palaeogeography, Palaeoclimatology, Palaeoecology*, *202*(1–2), 143–152. http://doi.org/10.1016/S0031-0182(03)00633-3

Mulitza, S., Chiessi, C. M., Cruz, A. P. S., Frederichs, T. W., Gomes, J. G., Gurgel, M. H. C., et al. (2013). Response of Amazon sedimentation to deforestation, land use and climate variability. Cruise No. MSM20/3 (February 19–March 11, 2012), Recife (Brazil)–Bridgetown (Barbados). MARIA S. MERIAN-Berichte, MSM20/3. DFG Senatskommission für Ozeanographie (86 pp.). http://doi.org/10.2312/cr_msm20_3

Mulitza, S., Chiessi, C. M., Schefuß, E., Lippold, J., Wichmann, D., Antz, B., et al. (2017). Synchronous and proportional deglacial changes in Atlantic meridional overturning and northeast Brazilian precipitation. *Paleoceanography*, *32*, 622–633. https://doi.org/10.1002/2017PA003084

Mulitza, S., Dürkoop, A., Hale, W., Wefer, G., & Niebler, H. S. (1997). Planktonic foraminifera as recorders of past surface-water stratification. *Geology*, *25*(4), 335–338. https://doi.org/10.1130/0091-7613(1997)025<0335:PFAROP>2.3.CO;2

Mulitza, S., Prange, M., Stuut, J. B., Zabel, M., Von Dobeneck, T., Itambi, A. C., et al. (2008). Sahel megadroughts triggered by glacial slowdowns of Atlantic meridional overturning. *Paleoceanography*, *23*, PA4206. https://doi.org/10.1029/2008PA001637

Murphy, S. J., Hurlburt, H. E., & O'Brien, J. J. (1999). The connectivity of eddy variability in the Caribbean Sea, the Gulf of Mexico, and the Atlantic Ocean. *Journal of Geophysical Research*, *104*(C1), 1431–1453. https://doi.org/10.1029/1998JC900010

Nace, T. E., Baker, P. A., Dwyer, G. S., Silva, C. G., Rigsby, C. A., Burns, S. J., et al. (2014). The role of North Brazil Current transport in the paleoclimate of the Brazilian Nordeste margin and paleoceanography of the western tropical Atlantic during the late Quaternary. *Palaeogeography, Palaeoclimatology, Palaeoecology*, *415*, 3–13. http://doi.org/10.1016/j.palaeo.2014.05.030

North Greenland Ice Core Project members (2004). High-resolution record of Northern Hemisphere climate extending into the last interglacial period. *Nature*, *431*(7005), 147–151. http://doi.org/10.1038/nature02805

Oudot, C., Morin, P., Baurand, F., Wafar, M., & Le Corre, P. (1998). Northern and southern water masses in the equatorial Atlantic: Distribution of nutrients on the WOCE A6 and A7 lines. *Deep-Sea Research Part I: Oceanographic Research Papers*, *45*(6), 873–902. https://doi.org/10.1016/S0967-0637(98)00002-8

Portilho-Ramos, R. C., Chiessi, C. M., Zhang, Y., Mulitza, S., Kucera, M., Siccha, M., et al. (2017). Coupling of equatorial Atlantic surface stratification to glacial shifts in the tropical rainbelt. *Scientific Reports*, *7*(1), 1561–1568. http://doi.org/10.1038/s41598-017-01629-z

Regenberg, M., Steph, S., Nürnberg, D., Tiedemann, R., & Garbe-Schönberg, D. (2009). Calibrating mg/ca ratios of multiple planktonic foraminiferal species with δ^{18}O-calcification temperatures: Paleothermometry for the upper water column. *Earth and Planetary Science Letters*, *278*(3-4), 324–336. http://doi.org/10.1016/j.epsl.2008.12.019

Reimer, P. J., Bard, E., Bayliss, A., Beck, J. W., Blackwell, P. G., Ramsey, C. B., et al. (2013). IntCal13 and Marine13 radiocarbon age calibration curves 0–50,000 years cal BP. *Radiocarbon*, *55*(04), 1869–1887. https://doi.org/10.2458/azu_js_rc.55.16947

Richardson, P. L., & Reverdin, G. (1987). Seasonal cycle of velocity in the Atlantic north Equatorial Countercurrent as measured by surface drifters, current meters, and ship drifts. *Journal of Geophysical Research*, *92*(C4), 3691–3708. https://doi.org/10.1029/JC092iC04p03691

Ridley, D. A., Heald, C. L., & Prospero, J. M. (2014). What controls the recent changes in African mineral dust aerosol across the Atlantic? *Atmospheric Chemistry and Physics*, *14*(11), 5735–5747. http://doi.org/10.5194/acp-14-5735-2014

Rind, D. H. (1998). Latitudinal temperature gradients and climate change. *Journal of Geophysical Research*, *103*(D6), 5943–5971. https://doi.org/10.1029/97JD03649

Rodrigues, R. R., Rothstein, L. M., & Wimbush, M. (2007). Seasonal variability of the south equatorial current bifurcation in the Atlantic Ocean: A numerical study. *Journal of Physical Oceanography*, *37*(1), 16–30. http://doi.org/10.1175/JPO2983.1

Rühlemann, C., Diekmann, B., Mulitza, S., & Frank, M. (2001). Late Quaternary changes of western equatorial Atlantic surface circulation and Amazon lowland climate recorded in Ceará Rice deep-sea sediments. *Paleoceanography*, *16*(3), 293–305. https://doi.org/10.1029/1999PA000474

Santos, T. P., Lessa, D. O., Venancio, I. M., Chiessi, C. M., Mulitza, S., Kuhnert, H., et al. (2017). Prolonged warming of the Brazil Current precedes deglaciations. *Earth and Planetary Science Letters*, *463*, 1–12. http://doi.org/10.1016/j.epsl.2017.01.014

Schlitzer, R. (2017). Ocean Data View, odv.awi.de.

Schneider, R. R., Müller, P. J., & Ruhland, G. (1995). Late Quaternary surface circulation in the east equatorial South Atlantic: Evidence from Alkenone Sea surface temperatures. *Paleoceanography*, *10*(2), 197–219. https://doi.org/10.1029/94PA03308

Schulz, M., & Mudelsee, M. (2002). REDFIT: Estimating red-noise spectra directly from unevenly spaced paleoclimatic time series. *Computers and Geosciences*, *28*(3), 421–426. http://doi.org/10.1016/S0098-3004(01)00044-9

Shakun, J. D., Clark, P. U., He, F., Marcott, S. A., Mix, A. C., Liu, Z., et al. (2012). Global warming preceded by increasing carbon dioxide concentrations during the last deglaciation. *Nature*, *484*(7392), 49–54. http://doi.org/10.1038/nature10915

Steph, S., Regenberg, M., Tiedemann, R., Mulitza, S., & Nürnberg, D. (2009). Stable isotopes of planktonic foraminifera from tropical Atlantic/Caribbean core-tops: Implications for reconstructing upper ocean stratification. *Marine Micropaleontology*, *71*(1–2), 1–19. http://doi.org/10.1016/j.marmicro.2008.12.004

Stocker, T. F. (1998). The seesaw effect. *Science*, *282*(5386), 61–62. http://doi.org/10.1126/science.282.5386.61

Stramma, L., Fischer, J., & Reppin, J. (1995). The North Brazil Undercurrent. *Deep-Sea Research Part I*, *42*(5), 773–795. http://doi.org/10.1016/0967-0637(95)00014-W

Stuut, J. B. W., Prins, M. A., Schneider, R. R., Weltje, G. J., Fred Jansen, J. H., & Postma, G. (2002). A 300-kyr record of aridity and wind strength in southwestern Africa: Inferences from grain-size distributions of sediments on Walvis ridge, SE Atlantic. *Marine Geology*, *180*(1–4), 221–233. http://doi.org/10.1016/S0025-3227(01)00215-8

Thomson, D. J. (1990). Time series analysis of Holocene climate data. *Philosophical Transactions of the Royal Society A: Mathematical, Physical and Engineering Sciences*, *330*(1615), 601–616. http://doi.org/10.1098/rsta.1990.0041

Veres, D., Bazin, L., Landais, A., Toyé Mahamadou Kele, H., Lemieux-Dudon, B., Parrenin, F., et al. (2013). The Antarctic ice core chronology (AICC2012): An optimized multi-parameter and multi-site dating approach for the last 120 thousand years. *Climate of the Past*, *9*(4), 1733–1748. https://doi.org/10.5194/cp-9-1733-2013

Vink, A., Rühlemann, C., Zonneveld, K. A. F., Mulitza, S., Hüls, M., & Willems, H. (2001). Shifts in the position of the north equatorial current and rapid productivity changes in the western tropical Atlantic during the last glacial. *Paleoceanography*, *16*(5), 479–490. https://doi.org/10.1029/2000PA000582

Wang, X., Auler, A. S., Edwards, L. L., Cheng, H., Cristalli, P. S., Smart, P. L., et al. (2004). Wet periods in northeastern Brazil over the past 210 kyr linked to distant climate anomalies. *Nature*, *432*(7018), 740–743. http://doi.org/10.1038/nature03067

Wefer, G., & Fischer, G. (1993). Seasonal patterns of vertical particle flux in equatorial and coastal upwelling areas of the eastern Atlantic. *Deep-Sea Research Part I*, *40*(8), 1613–1645. http://doi.org/10.1016/0967-0637(93)90019-Y

Wejnert, K. E., Thunell, R. C., & Astor, Y. (2013). Comparison of species-specific oxygen isotope paleotemperature equations: Sensitivity analysis using planktonic foraminifera from the Cariaco Basin, Venezuela. *Marine Micropaleontology*, *101*, 76–88. http://doi.org/10.1016/j.marmicro.2013.03.001

Weldeab, S., Schneider, R. R., & Kölling, M. (2006). Deglacial sea surface temperature and salinity increase in the western tropical Atlantic in synchrony with high latitude climate instabilities. *Earth and Planetary Science Letters*, *241*(3–4), 699–706. http://doi.org/10.1016/j.epsl.2005.11.012

Williams, D. F., & Healy-Williams, N. (1980). Oxygen isotopic-hydrographic relationships among recent planktonic foraminifera from the Indian Ocean. *Nature*, *283*(5750), 848–852. http://doi.org/10.1038/283848a0

Wolff, E. W., Chappellaz, J., Blunier, T., Rasmussen, S. O., & Svensson, A. (2010). Millennial-scale variability during the last glacial: The ice core record. *Quaternary Science Reviews*, *29*(21–22), 2828–2838. http://doi.org/10.1016/j.quascirev.2009.10.013

Wolff, T., Mulitza, S., Rühlemann, C., & Wefer, G. (1999). Response of the tropical Atlantic thermocline to late Quaternary trade wind changes. *Paleoceanography*, *14*(3), 374–383. https://doi.org/10.1029/1999PA900011

Zhang, Y., Chiessi, C. M., Mulitza, S., Sawakuchi, A. O., Häggi, C., Zabel, M., et al. (2017). Different precipitation patterns across tropical South America during Heinrich and Dansgaard-Oeschger stadials. *Quaternary Science Reviews*, *177*, 1–9. http://doi.org/10.1016/j.quascirev.2017.10.012

Zhang, Y., Chiessi, C. M., Mulitza, S., Zabel, M., Trindade, R. I. F., Hollanda, M. H. B. M., et al. (2015). Origin of increased terrigenous supply to the NE south American continental margin during Heinrich Stadial 1 and the younger Dryas. *Earth and Planetary Science Letters*, *432*, 493–500. http://doi.org/10.1016/j.epsl.2015.09.054